1   **SHEAR CAPACITY OF UNBONDED POST-TENSIONED CONCRETE T-BEAMS**

2   **STRENGTHENED WITH CFRP AND GFRP U-WRAPS**

3   Long Nguyen-Minh[1], Dien Vo-Le[2], Duong Tran-Thanh[3], Thong M. Pham[4], Chinh Ho-Huu[5],

4   Marián Rovňák[6]

5

6   **ABSTRACT**

7   Existing codes and design guidelines have not mentioned a procedure to calculate the shear

8   resistance of unbonded post-tensioned concrete beams strengthened with fiber reinforced

9   polymer (FRP) sheets. Up to date, the number of studies about the shear behaviour of post-

10   tensioned concrete beams strengthened with FRP sheets in shear is very limited, particularly

11   for unbonded post-tensioned beams. The effect of many factors on the shear resistance of

12   such the beams has not been well investigated, for example, fiber factors (the type of fiber,

13   the strengthening scheme, and the number of layers), the concrete strength, and the ratio of

14   the shear span to effective depth. The study deals with the shear behaviour of unbonded post-

15   tensioned beams strengthened with FRP U-wraps. The experiment consists of twenty-two

16   post-tensioned beams with T section and unbonded tendons. The variables include concrete

17   strength, number of FRP layers, FRP U-wraps scheme (continuous and spaced), types of FRP,

18   and varied shear span to effective depth. The experimental results have shown that the FRP

[1] Assoc. Professor, Department of Structural Design, Faculty of Civil Engineering, HCMC University of Technology, 268 Ly Thuong Kiet, District 10, Ho Chi Minh city, Vietnam; Ph.D., Faculty of Civil Engineering, Technical University of Košice, Letná 9, 042 00 Košice, Slovakia. E-mail: nguyenminhlong@hcmut.edu.vn (corresponding author)
[2] Ph.D. Student, Department of Structural Design, Faculty of Civil Engineering, HCMC University of Technology, 268 Ly Thuong Kiet, District 10, Ho Chi Minh city, Vietnam, E-mail: voledien@gmail.com
[3] BK Structural Engineering Lab, Faculty of Civil Engineering, HCMC University of Technology, 268 Ly Thuong Kiet, District 10, Ho Chi Minh city, Vietnam; E-mail: tranthanhduong31@ gmail.com.
[4] Research Fellow, PhD., Centre for Infrastructural Monitoring and Protection, School of Civil and Mechanical Engineering, Curtin University, Australia; Lecturer, Department of Structural Design, Faculty of Civil Engineering, HCMC University of Technology, 268 Ly Thuong Kiet, District 10, Ho Chi Minh city, Vietnam. E-mail:thong.pham@curtin.edu.au.
[5] Lecturer, PhD., Department of Structural Design, Faculty of Civil Engineering, HCMC University of Technology, 268 Ly Thuong Kiet, District 10, Ho Chi Minh city, Vietnam, E -mail: c.hohuu@hcmut.edu.vn.
[6]Assoc. Professor, Ph.D., Department of Masonry and Concrete Structures, Faculty of Civil Engineering; Technical University of Košice, Letná 9, 042 00 Košice, Slovakia. E-mail: marian.rovnak@tuke.sk

shear strengthening is more effective with higher concrete strength. The number of FRP layers, strengthening scheme, and type of FRP have a slight influence on the shear resistance of the beams but they significantly affect the ultimate deformation of the FRP sheets. The efficiency of FRP U-wraps considerably reduces with a reduction of the shear span to effective depth. As a result, the existing design guides may not yield reliable predictions since they have not considered this ratio. Moreover, a semi-empirical model is proposed to predict the shear resistance of unbonded post-tensioned beams strengthened with FRP U-wraps. The predictions from the proposed model fit well with the experimental results from other studies.

Keywords: concrete strength; shear span; fabric-epoxy U-wrap; unbonded tendons; post-tensioned beam; shear capacity; formula.

INTRODUCTION

Externally bonded FRP strengthening systems to improve the shear resistance of reinforced concrete (RC) or prestressed concrete (PC) members have been commonly used and have demonstrated its high efficiency. However, understanding the true mechanism of the shear behaviour is always a challenging task for not only structural engineers but also the research society. Previous studies have shown that properly evaluating the shear resistance of RC beams strengthened with FRP sheets is complicated because of the interaction of some factors, for instance, the stirrups ratio, the FRP shear reinforcement ratio, the strengthening scheme, the beam geometry, the concrete strength, and the ratio of the shear span to effective depth as presented by Khalifa and Nanni (2000), Deniaud and Cheng (2001), Bousselham and Chaallal (2004), Pellegrino and Modena (2006), Perera et al. (2010), Chen et al. (2012, 2016), Dias and Barros (2013), Nguyen–Minh and Rovňák (2015), Dror and Rabinovitch (2016), Mostofinejad et al. (2016), Colotti (2016), and Li and Leung (2015, 2017). The understanding about the shear mechanism of PC beams strengthened with FRP sheets is even more limited because there are only a few studies available in the literature (Reed and

Peterman, 2004; Kim et al. 2012; Kang and Ary, 2012; Murphy et al. 2012, and Nguyen et al. 2016). In addition, the mentioned previous studies only investigated the shear mechanism of pre-tensioned concrete beams strengthened with FRP sheets and there is no study investigating the shear mechanism of unbonded post-tensioned concrete (UPC) beams strengthened with FRP sheets. The effect of some factors, such as the concrete strength, the shear span-to-depth ratio, the thickness of FRP sheets, the strengthening scheme, and especially the use of GFRP sheets, to the shear resistance of such beams has not been comprehensively investigated. Contrary to the prestressed pre-tensioned concrete beams, in which bonded tendons and surrounding concrete maintain the integrity, and thus the strain compatibility between tendons and concrete is satisfied, the interaction of unbonded tendons and concrete does not exist along the post-tensioned beams, which, consequently, could lead to a reduction of the FRP shear-strengthening efficiency of UPC beams comparing to that of PC beams.

The current design guides and codes (ACI 440.2R, 2008; NCHRP 678, 2011; TR55, 2012; and CNR DT 200R1, 2013) have not provided a procedure to predict the shear resistance of UPC beams strengthened with FRP sheets because of the lack of experimental studies about this topic. Moreover, analytical models in the design guides for the shear behaviour of RC beams or PC beams strengthened with FRP sheets were derived based on experimental results of RC beams strengthened with FRP sheets. These models adopted the superposition theorem and separately considered the contributions of concrete, stirrups, and FRP sheets while the interaction between these components and the effect of the shear span-to-depth ratio were ignored. Previous studies have shown that there is an interaction between these factors in which the shear span-to-depth ratio affected the angle of inclined cracks and the deformation of FRP sheets was influenced by the bonding between the FRP sheets and concrete surface (Bousselham and Chaallal, 2006; Al-Rousan and Issa, 2016; Li and Leung, 2015, 2017). The

1 prestress results in more brittle behaviour in comparison with that of RC beams. This change

2 in the structural behaviour affects the shear resistance of the compressive concrete zone,

3 reduces the tensile stress of concrete in the inclined direction, closes cracks, increases the

4 interlock effect of aggregates, and thus changes the deformation field of the FRP sheets in

5 shear span. Therefore, it is necessary to propose a new model to predict the shear resistance

6 of PC beams and especially UPC beams strengthened with FRP sheets, in which it reflects the

7 interaction of main its components.

8 This study investigates the shear behavior of UPC beams strengthened with FRP U-wraps.

9 The variables include three concrete strengths, two numbers of FRP layers, FRP U-wrap

10 schemes (continuous and spaced), two types of FRP, and varied shear span-to-depth ratio.

11 The objective of this study is to investigate the effect of the above variables to the shear

12 beahvior of the beams. In addition, a new model is proposed to predict the shear resistance of

13 UPC beams strengthened with FRP sheets.

14 **EXPERIMENTAL INVESTIGATION**

15 *Materials*

16 The tested beams were cast by concrete of three different strength classes (groups A, B, and

17 C), which had compositions of: cement PC40, river sand 0-4 mm, coarse aggregates 20-22

18 mm, fine aggregates 2 mm, water, and plasticizer. The mixture design of the three groups is

19 listed in order as follows: group A (400 kg/m^3, 530 kg/m^3, 1045 kg/m^3, 227 kg/m^3, 182 l/m^3,

20 and 4.8 l/m^3); group B (420 kg/m^3, 560 kg/m^3, 1017 kg/m^3, 240 kg/m^3, 170 l/m^3, and 6.3

21 l/m^3); and group C (460 kg/m^3, 549 kg/m^3, 998 kg/m^3, 235 kg/m^3, 170 l/m^3, and 6.9 l/m^3),

22 respectively.

23 The compressive strength ($f_{c,cube}$) and the splitting strength ($f_{sp,cube}$) were determined from 6

24 concrete cubes 150x150x150 mm and the results are presented as follows: group A, $f_{c,cube}$ =

25 38.3 MPa and $f_{sp,cube}$ = 3.9 MPa; group B, $f_{c,cube}$= 55.5 MPa and $f_{sp,cube}$= 6.9 MPa; group C

$f_{c,cube}$= 73.4 MPa and $f_{sp,cube}$= 8.6 MPa. The slumps of concete of groups A, B, and C were 135 mm, 120 mm, and 105 mm, respectively.

The yield strength and ultimate strength of the reinforcements averaged from three samples were f_y= 430 MPa and f_u= 600 MPa, respectively, for longitudinal rebars and f_{yw}= 342 MPa and f_{uw}= 463 MPa, respectively, for stirrups. Young modulus (E_s) of the reinforcements was 200 GPa.

Tendons consisted of seven-wire strands with the nominal diameter of 15.2 mm, the nominal yield strength and ultimate strength of 1675 MPa and 1860 MPa, respectively. Young modulus of the tendons was E_p = 196 GPa. The nominal thicknesses of 1 layer of CFRP and GFRP sheets (**Fig. 1**) were 1.0 mm and 1.3 mm, respectively. The mechanical properties of concrete, tendons, reinforcements, and FRP sheets are summarized in **Table 1**.

Test specimens

In total, twenty-two UPC test beams of the same T-section and span were proposed as follows: the cross-section height (h) of 500 mm; the flange width (b_f) of 300 mm; the flange thickness (h_f) of 80 mm; the web thickness (b) of 120 mm; the total beam length (L_0) of 3500 mm, and the effective beam span (L) of 3200 mm.

Each beam was post-tensioned by two straight tendons of nominal diameter of 15.2 mm. Tensile longitudinal reinforcement consists of two rebars of 25 mm in diameter and four rebars of 12 mm in diameter were placed at the compression side. The stirrups, which were uniformly distributed along the beams except near the two ends of the beams, were plain round bars with diameter of 6 mm and the spacing of 300 mm. To avoid the local damage at the two ends of the beams (200 mm), the stirrups were placed with the spacing of 50 mm.

Twenty-two UPC test beams were divided into three groups A, B, and C of varying concrete strengths (group A − $f_{c,cube}$ = 38.3 MPa; group B − $f_{c,cube}$ = 55.5 MPa; group C − $f_{c,cube}$ = 73.4 MPa). Each of groups A and C includes one beam without strengthening (reference beam)

1   and seven beams strengthened with FRP sheets consiting of five beams wrapped with CFRP

2   (three beams were strengthened with two-layer spaced U-wraps, one beam with one-layer

3   spaced U-wraps, and last one with one layer of continuous U-wraps), and two beams were

4   wrapped with GFRP (one beam was strengthened with one-layer spaced U-wraps and another

5   one with one-layer continuous U-wraps). Group B consisted of 6 beams including one

6   reference beam, three beams strengthened with CFRP (one beam was strengthened with one-

7   layer spaced U-wraps, the second one with two-layers spaced U-wraps, and the third one with

8   one layer of continuous U-wraps), and two remaining beams were strengthened with GFRP

9   (first beam was strengthened with one-layer spaced U-wraps and second one with one-layer

10   continuous U-wraps).

11   Details of the beam geometry and the mechanical properties of tendons, reinforcements, and

12   FRP are listed in **Table 2**. The beam section, arrangement of tendons, reinforcements, and

13   strengthening schemes are shown in **Figs. 2 and 3**.

14   After the curing period of 28 days, the beams were prestressed by unbonded tendons. The

15   initial applied force in each tendon, F_{pi}, was 182.3 kN which resulted in the corresponding

16   compressive stress in concrete f_{pc} =4.6MPa. It is noted that these beams were designed

17   according to ACI 318 (2014) for class U and without cracks. As a result, the initial force was

18   determined in order to meet the condition $f_t < 0.62(f_c')^{0.5}$, at which f_t is the the maximum

19   tensile stress in concrete and f_c' is the compressive concrete strength from cylinders. All the

20   beams in this study were satisfied the above condition, for example, group A (lowest concrete

21   strength $f_{c,cube}$ =38.3MPa) had f_t =1.34MPa < $0.62(f_c')^{0.5}$ =3.84MPa and groups B and C with

22   higher concrete strength also passed the above condition.

23   Before bonding with FRP sheets, the concrete surface was ground with an angle grinder until

24   touching aggregates. Any holes or imperfection on the concrete surface were filled with

25   epoxy and then ground off. A vacuum cleaner was used to clean any dust on the concrete

1   surface which also was checked again carefully before bonding. Epoxy was mixed according

2   to the instruction provided by a manufacturer and a thin layer of epoxy was spread on the

3   concrete surface by a roller before placing the first layer of the FRP sheet. Another epoxy

4   layer was then spread on the top of the first FRP sheet while just-enough pressure was

5   applied via the roller so that the FRP sheet was saturated. The roller was rolled gently on top

6   of the applied FRP sheets to ensure there was no air bubble in the composite matrix. The

7   wrapping process was carried out in the laboratory at the average temperature of 29°C and the

8   humidity of 75%. The strengthened beams were left in the laboratory for 7 days during the

9   curing period to ensure developing the full strength of the epoxy.

10   *Test procedure and instrumentation*

11   The beams were tested under four point bending tests as shown in **Figs. 3c and 3d**. All test

12   beams have the same shear span-to-depth ratio $a/d_e = 2.3$ except three beams strengthened

13   with two layer spaced CFRP U-wraps of each group A (P-A2-2.3-C, P-A2-1.9-C, and P-A2-

14   1.5-C) and group C (P-C2-2.3-C, P-C2-1.9-C, and P-C2-1.5-C). These beams were tested

15   with ratio $a/d_e = 2.3$, 1.9, and 1.5, respectively, in order to assess effect of shear span to shear

16   behavior of the beams.

17   Five linear variable differential transformers (LVDT) were utilized to measure the

18   displacement of the beams at the midspan, the applied load locations, and the supports. The

19   strain of FRP sheets was determined by using 10 strain gauges (SG) which were uniformly

20   distributed within the shear span region of the beam as shown in **Figs. 3c** and **3d**. The strain

21   in tendons was monitored via two SGs bonded at the midspan and within the shear span as

22   shown in **Fig. 2a**. Similarly, two other SGs were bonded to the longitudinal reinforcements at

23   the midspan and in the shear span to measure the strain of these reinforcements while the

24   strain of stirrups were monitored by two SGs bonded to the two legs of stirrups in the shear

25   span (**Fig. 2a**). Meanwhile, the compressive strain of concrete was measured by total five

1 SGs: three SGs at midspan and two other SGs at two loading points as shown in **Fig. 3c** and **d**.

2 The beams were loaded by a hydraulic jack with the capacity of 1000 kN and the force

3 control mode was used with the loading rate of 15 kN/min. At each loading step (between 30

4 kN to 50 kN), all measurement, including the displacement of the beam, strain of FRP sheets,

5 tendons, reinforcements, concrete, the crack occurrence and its development, were recorded.

6 **TEST RESULTS AND DISCUSSION**

7 ***Failure of specimens***

8 The experimental results are summarized in **Table 3**. All the tested beams failed in the shear

9 behaviour with crushing of the concrete at the loading points. It should be noted that the

10 actual first crack occurred as a flexural vertical crack between the two loading points. When

11 the applied load increased, the existing cracks opened and new cracks appeared towards the

12 supports in the shear span. Once one of them started clearly in direction inclined to the

13 horizontal beam axis, it was considered as the first inclined crack in the shear span and load

14 force value was defined as $P_{cr,sh}$.

15 The first inclined crack in the reference beam appeared at the loading level $P_{cr,sh}/P_{u,tot,exp}$ =

16 0.34, at which $P_{cr,sh}$ is the applied force corresponding to the first inclined crack and $P_{u,tot,exp}$

17 is the ultimate applied load of the beam. In the meantime, the first inclined crack in the

18 strengthened beam occurred later at the greater averaged applied load $P_{cr,sh}/P_{u,tot,exp}$ = 0.4. The

19 values of $P_{cr,sh}$ of the beams P-A1-2.3-C-Cont, P-B1-2.3-C-Cont, and P-C1-2.3-C-Cont were

20 not presented in **Table 3** because these beams were strengthened by CFRP jackets of black

21 colour which prevented the identification of the first crack.

22 The thickness of the FRP sheets and the shear span ratio a/d_e had a slight influence on the

23 ratio $P_{cr,sh}/P_{u,tot,exp}$ while the concrete strength, type of FRP (CFRP or GFRP) and

24 strengthening scheme (continuous or spaced) did not show a noticeable influence on this ratio.

25 The debonding of the FRP sheets locally occurred at the FRP sheets at the middle of the shear

8

span and was associated with a cracking sound at the loading level $P_{u,deb}/P_{u,tot,exp} = 0.79 - 0.92$ in which $P_{u,deb}$ is the applied load when the first cracking sound was heard. Before full debonding of the CFRP sheets, the local debonding adjacent to the inclined cracks accompanying with cracking sounds was observed. Corresponding load forces, approximately $P= (0.79{\sim}0.90) P_u$, were defined as debonding forces $P_{u,deb}$.

When the applied load was approaching the ultimate load, the FRP sheets suddenly debonded associated with a thin concrete layer attached to the sheets and an explosive sound. There has not been a clear correlation of the ratio $P_{u,deb}/P_{u,tot,exp}$ as well as debonding mode of FRP sheets with the investigated variables, such as, the concrete strength, type of FRP (CFRP or GFRP), strengthening scheme (continuous or spaced), thickness of FRP sheets, and the shear span ratio a/d_e. The failure of the unstrengthened beams was very brittle associated with an explosive sound and 2-3 major cracks. The higher concrete strength was used, the louder explosive sound was heard. In the other hand, the strengthened beams failed with a lower rate associated with a major crack because of the use of the FRP sheets. The width of the major cracks was about 4-5 mm for both strengthened and unstrengthened beams, in which FRP sheets significantly changed the failure angle. The angle of cracks (angle of crack inclination respect to the beam axis) in the unstrengthened beams was about 25.6-28.7º while the corresponding one of the strengthened beams was approximately 26.3-40.3º. The angle of the inclined crack of the beams strengthened with continuous FRP U-wraps was greater than that of the beams strengthened with spaced FRP U-wraps. In general, the crack angle tended to slightly increase with the increase of concrete strength. The crack angle significantly increased with a reduction of the shear span ratio a/d_e, for example, the angle increased from 31.9º to 38.8º for group A and from 35.8º to 40.3º for group C when the shear span ratio a/d_e reduced from 2.3 to 1.5. The failure modes and cracks of the tested beams are shown in **Fig. 4**.

1   *Load-displacement responses, shear cracking behavior, and shear resistance*

2   The typical load-displacement curves of the tested beams are presented in **Fig. 5** while the

3   applied load and ultimate displacement are summarized in **Table 3**. In general, the shear

4   behaviour of the tested beams can be classified into two stages including before and after the

5   occurrence of the first inclined crack. Before the occurrence of the first inclined crack ($P <$

6     $0.34P_{u,tot,exp}$ for the reference beam and $< 0.4P_{u,tot,exp}$ for the strengthened beams), all the

7   beams behaved in a linear manner and there was no difference between them. During this

8   period, the effect of FRP sheets on the shear behaviour was negligible. After the occurrence

9   of the first inclined crack ($P > 0.34P_{u,tot,exp}$ for the reference beam and $>0.4P_{u,tot,exp}$ for the

10   strengthened beams), the tested beams did not show a pure linear behaviour and the beam

11   behaviour gradually changed to a non-linear manner, especially the behaviour of FRP

12   strengthened beams. The contribution of the FRP sheets was activated and the sheets carried

13   a portion of the principal tensile stress in the shear span, which slowed down the formation of

14   the inclined cracks and increased the shear-cracking force by 20% to 40% averagely as

15   shown in **Fig. 6**. This increase was proportional to the concrete strength and the number of

16   FRP layers. This mechanism also slowed down the degradation of the stiffness of the

17   strengthened beams as compared to those of the reference beams. As a result, the

18   displacement of the strengthened beams was smaller than that of the reference beams at the

19   same load (**Fig. 5**). This trend was more obvious with higher concrete strength, for example,

20   at the ultimate load of the reference beams, the average displacement reduction of the

21   strengthened beams compared to the reference beams was approximately 14% for group A,

22   18% for group B, and 39% for group C. The continuous FRP U-wraps showed a better ability

23   to slow down the stiffness reduction rate of the beams as compared to the spaced FRP U-

24   wraps, and thus the displacement increasing rate of the beams strengthened with continuous

25   FRP U-wraps was smaller than those strengthened with spaced FRP U-wraps. However, the

strengthened beams showed the maximum displacement much greater (1.06 to 1.7 times) than those of the reference beams as shown in **Fig. 7**. The most effective strengthening scheme was the continuous FRP U-wraps and CFRP strengthened beams showed higher maximum displacement as compared to GFRP strengthened beams.

The FRP sheets improved the shear resistance of the tested beams from 6% - 26% and this enhancement increased with the concrete strength (**Fig. 7**). The shear enhancement observed in this study was quite similar to those in the literature, for example, the shear enhancement of 7% - 29% was reported by Hutchinson et al. (1998) and Reed and Peterman (2004) for pre-tensioned concrete T-beams strengthened with CFRP. It is noted that the efficiency of using FRP increases with the concrete strength. This higher efficiency is attributed to the better bonding strength between FRP sheets and higher strength concrete as suggested by Chajes et al. (1996) and Guo et al. (2005). The increase in the bonding strength led to a rise in the strain of FRP sheets as reported in **Table 3**, which in turn improved the efficiency of using FRP reinforcement. For the tested beams in the three groups in this study, the efficiency of using CFRP sheets was approximately 5% higher than that of GFRP sheets although the stiffness of the first one was equal to 2.8 times the stiffness of the later one $[(t_f \times E_f)_{CFRP}/(t_f \times E_f)_{GFRP} = (1.0 \times 95.8)/(1.3 \times 26.1) = 2.8]$. This observation has shown that the effect of different types of FRP to the shear resistance of strengthened UPC beams was marginal. In addition, a study on the shear resistance of typical RC beams strengthened with CFRP/GFRP sheets also found the same observation (Nguyen–Minh and Rovňák, 2015). In that study, the shear resistance of RC beams strengthened with CFRP sheets was about 12% greater than that of beams strengthened with GFRP sheets. Interestingly, the experimental results in **Table 3** showed a marginal difference (5%) between the debonding forces, $P_{u,deb}$, in the cases of CFRP strengthened beams and GFRP strengthened beams $[(P_{u,deb,CFRP} - P_{u,deb,GFRP})/P_{u,deb,GFRP} \approx 5\%]$, which was equal to the difference (5%) in the ultimate load between two types of the beams.

1 The marginal difference between the debonding force of CFRP strengthened beams and

2 GFRP strengthened beams explain the minor enhancement of beams strengthened with CFRP

3 sheets as compared to those with GFRP sheets.

4 In general, considering the same CFRP sheet ratio, using continuous CFRP U-wraps showed

5 a better performance than spaced FRP U-wraps in shear resistance aspect but the

6 enhancement was small (about 6~7%). The shear resistance of the CFRP strengthened beams

7 increased with a reduction of the shear span ratio a/d_e (**Fig. 8**). For example, when the shear

8 span ratio a/d_e reduced from 2.3 to 1.9 and from 2.3 to 1.5, the average improvement in shear

9 resistance of the strengthened beams was 12% and 28%, respectively. This trend was not

10 affected by the concrete strength.

11 ***Strain in FRP sheets and stirrups***

12 The relationships between the applied load and the strain of FRP sheets or stirrups of the

13 tested beams are presented in **Fig. 9** while the maximum strain of FRP sheets and stirrups are

14 summarized in **Table 3**. The positions of SGs bonded to FRP sheets and stirrups are shown in

15 **Figs. 2** and **3**. The behaviour of FRP sheets and stirrups is divided into two stages. Before the

16 occurrence of the first inclined crack ($P < 0.4P_{u,tot,exp}$), the strain of FRP sheets and stirrups

17 were very small and quite similar each other. The experimental results have shown that FRP

18 sheets and stirrups have not contributed to the shear resistance of the beams yet. After the

19 occurrence of the first inclined crack ($P > 0.4P_{u,tot,exp}$), the strain of both FRP sheets and

20 stirrups increased significantly with a fast rate at which the increasing rate of stirrup's strain

21 was faster than that of FRP sheets, indicating the contribution of stirrups was activated earlier

22 than that of FRP sheets. In addition, the increasing rate of continuous U-wraps was much

23 lower than that of spaced U-wraps.

24 The maximum strain of FRP sheets was dependent on type of FRP (CFRP or GFRP), the

25 strengthening scheme (continuous or spaced), the concrete strength, and the shear span ratio

1   a/d_e (**Fig. 10)**. The maximum strain of continuous CFRP U-wraps was quite small, ranging

2   between 2.29‰ and 3.64‰, which corresponds to approximately from 23% to 36% of the

3   rupture strain of CFRP sheets while the maximum strain of spaced CFRP U-wraps ranged

4   from 5.37‰ to 7.21‰ (approximately from 53% to 72% of the rupture strain), experiencing

5   an increase of 2-2.3 times as compared to that of continuous CFRP U-wraps. Similarly, the

6   maximum strain of continuous GFRP U-wraps was from 4.66‰ to 5.52‰, which

7   corresponds to approximately from 21% to 25% of the rupture strain of GFRP sheets while

8   the corresponding strain of spaced GFRP U-wraps were from 5.97‰ to 8.55‰

9   (approximately from 27% to 39% of the rupture strain), showing an increase of 1.3-1.5 times

10   in comparison with that of continuous GFRP U-wraps. These results have shown that the

11   limit strain = 4‰ according to ACI 440.2R (2008) was much conservative. This limit strain

12   should be adjusted particularly for spaced GFRP U-wraps in order to ensure economic aspect

13   of the design.

14   As expected, the higher concrete strength, the higher maximum FRP sheet strain. The greater

15   strain of FRP sheets in spaced U-wraps as compared to that in continuous U-wraps may be

16   resulted from the stress concentration phenomenon. Accordingly, spaced FRP U-wraps

17   intersecting with a crack showed a great number of strain while other FRP U-wraps

18   experienced much lower strain. On the other hand, the beams strengthened with continuous

19   U-wraps had more uniform strain in the FRP sheets so that the stress concentration and local

20   damage were mitigated and thus experienced lower maximum strain in FRP sheets as shown

21   in **Fig. 10**. With the same strengthening scheme, the maximum strain of GFRP sheets was

22   greater than that of CFRP sheets, for example, from 1.5 to 2 times for continuous U-wraps

23   and from 1.1 to 1.2 times for spaced U-wraps. These results agreed well with the

24   experimental study by Nguyen–Minh and Rovňák (2015) in which the strain of GFRP sheets

25   was nearly 1.3 times higher than that of CFRP sheets in RC beams strengthened with FRP.

13

1   The smaller maximum strain of CFRP sheets as compared to that of GFRP sheets was

2   attributed to their different stiffnesses. Moreover, the maximum strain of FRP sheets reduced

3   considerably with the reduction of the shear span ratio a/d_e (**Fig. 10**). When the shear span

4   ratio a/d_e reduced from 2.3 to 1.5, the maximum FRP sheet strain decreased by 24% for

5   Group A and 33% for Group C. This observation agreed well with the experimental results

6   reported by Li and Leung (2015). Meanwhile, the dependence of FRP sheet strain on the

7   shear span ratio was more obvious with higher concrete strength. The use of FRP sheets

8   becomes less effective in beams with smaller the shear span ratio. This phenomenon can be

9   attributed to the angle of inclined cracks, which are greater for shorter shear span ratio, to the

10   longitudinal axis of the beams (**Table 3**). Therefore, the angle between FRP sheets and the

11   inclined cracks is smaller for shorter shear span ratio beams, indicating the contribution of

12   FRP sheeets to the shear resistance of the beams will be smaller. Moreover, the smaller the

13   shear span ratio, the more dominant the arch effect in the beam, which leads to a lower

14   efficiency of the FRP strengthening.

15   The maximum strain of stirrups in the unstrengthened beams of Groups A, B, and C were

16   15.5‰, 16.7‰, and 17.8‰, respectively, which were greater than the yield strain of steel

17   (f_{yw}/E_s =345/200000= 1.73‰). On the other hand, the average maximum strain of stirrups in

18   the strengthened beams of groups A, B, and C were 9.5‰, 10.5‰, and 13.5‰, respectively,

19   which show a reduction of 1.69, 1.59, and 1.35 times as compared to the control beams, and

20   indicating thus the strongly interaction of stirrups and FRP sheets, reffered, however, for

21   strengthened RC beams by Bousselham and Chaallal (2004, 2006); Pellegrino and Modena

22   (2008); Chen et al. (2010, 2013); and Pellegrino and Vasic (2013).

23   ***Strain in tendons, rebars, and concrete***

24   The relationship between the load and the strain of tendons at the midspan in the tested beams

25   is shown in **Fig. 11**. At failure, the maximum strain of tendons at the midspan ranged

1   between 7.6‰ and 7.9‰ which was smaller than the yield strain (f_{py}/E_p =1675/196500 =

2   8.5‰) provided by the manufacturer so that these tendons did not yield (**Table 3**). The

3   maximum strain of tendons within the shear span was 2.4% smaller than that at the midspan.

4   Before the occurrence of the first inclined crack ($P < 0.4P_{u,tot,exp}$), the behaviour of tendons in

5   the all beams was similar. However, after the occurrence of the first inclined crack ($P >$

6     $0.4P_{u,tot,exp}$), the strain of tendons in the strengthened beams increased with a lower rate than

7   that of the unstrengthened beams. At the same load, for example, at the ultimate load of the

8   unstrengthened beams the strain of tendons in the strengthened beams was smaller than those

9   of the reference beams and these reductions were 16% for group A, 13% for group B, and

10   15.5% for group C, respectively. As mentioned previously, the FRP sheets governed the

11   crack formation and the crack development in shear span so that they in turn affected the

12   strain of tendons. This mechanism helps to avoid a sudden change of the beam stiffness when

13   cracks occur and it, therefore, slows down the increasing rate of the tendon strain in the

14   strengthened beams. Interestingly, at the ultimate stage, the maximum strain of tendons did

15   not show a considerable difference.

16   In the same manner, the FRP sheets affected strain in the longitudinal reinforcements, but the

17   influence was not as clear as the case of tendons. The increasing rate of strain of the

18   longitudinal reinforcements in the strengthened beams was slower than that in the reference

19   beams (**Fig. 12**). At the ultimate stage, the strain of the longitudinal reinforcements at the

20   midspan ranged from 2.21‰ to 3.39‰ which was greater than the yield strain (f_y/ E_s=

21   430/200000 = 2.15‰). However, the strain of the longitudinal reinforcements at the shear

22   span was small, ranging from 1.7‰ to 2‰ and corresponding to 80% to 90% the yield strain,

23   respectively. It indicated that longitudinal reinforcements in the shear span region did not

24   yield.

1 The maximum strain of concrete at the loading points ranged from 2.85‰ to 3.37‰, which

2 was 2.7 times greater than that at the midspan (**Table 3**). This difference in the concrete strain

3 might be caused by the stress concentration at the loading points. At the ultimate stage, the

4 experiment has shown that all the tested beams had concrete crushing at the loading points.

5 **THEORETICAL INVESTIGATION**

6 *Proposed formula*

7 The shear resistance of UPC beams strengthened with FRP materials is dependent on not only

8 each single factors, for example, the concrete strength, the initial post-tensioning force, the

9 trajectory of tendons, the beam geometry, and FRP sheets (type of fiber, strengthening

10 scheme, FRP ratio) but also the interaction between these factors. Empirical models presented

11 in the current codes (ACI 440.2R, 2008; TR55, 2012; and CNR DT 200R1, 2013) for

12 structures strengthened with external FRP sheets were derived based on the superposition

13 theorem in which the contribution of each component was individually considered. Especially,

14 these codes have just provided design procedures for PC beams using bonded tendons

15 strengthened with FRP sheets while there is no document mentioning a procedure for the

16 design of UPC beams strengthened with FRP sheets in shear. The proposed model needs to

17 satisfy the equilibrium conditions, strain compatibility, and material constitutive laws.

18 The free body diagram of a simply supported beam used in the proposed model is presented

19 in **Fig. 13**. The equilibrium of forces are presented in the following equations:

20
$$H_p + F_s = F_c \tag{1}$$

21
$$H_p \left[d_p - (x_{sh} - x_T) \right] + (V_F + V_S)\frac{a_T}{2} + F_s z_C + V_p a_T = V_{re}a \tag{2}$$

22 In Equation 1, the horizontal component of the force in tendons, H_p (N), is determined as

23 follows:

24
$$H_p = F_p \cos\theta \tag{3}$$

The experimental results in this study (**Table 3**) have shown that tendons in the tested beams did not yield so that the force in the tendons can be estimated as follows:

$$F_p = E_p \varepsilon_{ps} A_P n_P \qquad (4)$$

where E_p (MPa) and A_p (mm^2) are the Young modulus and cross section of the tendons; n_p is the number of tendons; ε_{ps} is the maximum strain in the tendons. In general, the strain in the tendons can not be estimated from the surrounding concrete since they do not have the integrity. The strain in the unbonded tendon, ε_{ps}, can be estimated as follows (Tam and Pannell, 1976):

$$\varepsilon_{ps} = \varepsilon_{pe} + \varphi \varepsilon_{c,\mathrm{sh}} \left(d_p - x_{sh} \right) / L \qquad (5)$$

where φ = 10.5 is the experimental coefficient (Tam and Pannell, 1976); ε_{pe}= f_{pe}/E_{ps}=$f_{pc}/(E_{ps} \times \rho_p)$ is the tendon strain after considering the prestress losses; f_{pc}=$\Sigma F/A_c$ (N/mm^2) is the effective prestress in concrete; ρ_p =A_p/A_c is the tendon ratio; F (N) is the effective prestressing force in one tendon; A_c (mm^2) is the cross section area; x_{sh} (mm) is the height of the compressive concrete zone at the ultimate stage; d_p (mm) is the depth to prestressed tendons; L (mm) is the span of beam; and θ is the angle of the tendon respect to the longitudinal axis of the beam (**Fig. 13**). The strain of concrete at the ultimate stage, $\varepsilon_{c,\mathrm{sh}}$, is equal to 0.003 as shown in the experimental restuls (**Table 3**).

Substituting Eqs. 4 and 5 into Eq. 3, the horizontal component of the force in the tendons, H_p, is calculated as follows:

$$H_p = E_{ps} A_P n_P \left[\varepsilon_{pe} + \varphi \varepsilon_{cu} \left(d_p - x_{sh} \right) / L \right] \cos \theta \qquad (6)$$

In Eq. 1, the force in the longitudinal reinforcements, F_s (N), is determined based on the assumption that the longitudinal reinforcements did not yield as shown in the experimental results. The results in **Table 3** have shown that the strain of the longitudinal reinforcements

1   varied from 80-93% of the yield strain. For the conservative purpose, the tension force in the

2   reinforcements is estimated about 80% of the yielding load:

3
$$F_s = 0.8 A_s f_y = 0.8 \rho_s b d_s f_y \tag{7}$$

4   where ρ_s is the steel ratio for the longitudinal reinforcements; f_y (MPa) is the yield strength of

5   the longitudinal reinforcements; d_s (mm) is the distance from the farest point of the

6   compressive region to the centroid of the longitudinal reinforcements; and b (mm) is the

7   width of the beam.

8   The compressive force in concrete, F_c (N), is estimated as follows:

9
$$F_c = b \int_0^{x_{sh}} \sigma_c dx \tag{8}$$

10   where the concrete strain is estimated from the equation proposed by Hognestad (1951):

11
$$\sigma_c(\varepsilon_c) = f_c' \left[2(\varepsilon_c / \varepsilon_0) - (\varepsilon_c / \varepsilon_0)^2 \right]; \tag{9}$$

12   where f_c' (MPa) is mean compressive strength of concrete cylinders; ε_o is the compressive

13   strain at peak stress:

14
$$\varepsilon_0 = 2 f_c' / E_c; \tag{10}$$

15
$$E_c = 4700 \sqrt{f_c'} \tag{11}$$

16   Assuming the linear strain diagram (**Fig. 13**), the compressive strain of concrete ε_c can be

17   expressed as:

18
$$\varepsilon_c = (\varepsilon_{c,sh} x) / x_{sh} \tag{12}$$

19   Substituting Eq.9 and Eq.12 into Eq. 8, the compression force in concrete, F_c, can be

20   expressed as:

21
$$F_c = b f_c' \left[\left(\frac{\varepsilon_{c,sh}}{\varepsilon_0} \right) x_{sh} - \left(\frac{\varepsilon_{c,sh}}{\varepsilon_0} \right)^2 \frac{x_{sh}}{3} \right] \tag{13}$$

1   Substituting Eqs. 6, 7, and 13 into Eq. 1 and using MatLab version 2015, the height of the

2   compressive concrete region, x_{sh}, can be approximated as (with variation about 3.9%):

3    $$x_{sh} = 25\left(f_c'\right)^{-1.07}\left(0.2f_{pc}+0.3\right)\left(\rho_s+0.015\right)b\left(d/10\right)^{1.1} \tag{14}$$

4   The length of the crack in the horizontal direction, a_T (mm), is expressed as (**Fig. 13**):

5    $$a_T = \left(d_p - x_{sh}\right)\big/\tan\alpha \tag{15}$$

6   where α (degree) is the angle of the crack respect to the longitudinal axis of the beam.

7   The distance x_T in Eq. (2) is given as follows (**Fig. 13**):

8    $$x_T = \left(\varepsilon_{cT}x_{sh}\right)\big/\varepsilon_{c,sh} \tag{16}$$

9   where ε_{cT} is the compressive strain of concrete at the centroid of the area under the stress–

10   strain diagram, which can be obtained when calculating the integral:

11   $$\varepsilon_{cT} = \left(\int_0^{\varepsilon_{c,sh}} \varepsilon_c\sigma_c d\varepsilon_c\right)\bigg/\left(\int_0^{\varepsilon_{c,sh}} \sigma_c d\varepsilon_c\right) \tag{17}$$

12   In Eq. 2, z_C is the lever arm of the internal forces (**Fig. 13**):

13   $$z_C = d_s - \left(x_{sh} - x_T\right) \tag{18}$$

14   The shear force across the compression zone V_c can be expressed in the form:

15   $$V_c = V_{re} - V_{sw} - V_p - V_F$$

16   (19)

17   where $V_p = F_p\sin\theta$.

18   In Eq. 2, the tension force in the FRP sheet, V_F, is determined as follows (ACI 440.2R, 2008):

19   $$V_F = \rho_f\varepsilon_{fe}E_f\left(\sin\beta+\cos\beta\right)b_w d_f \tag{20}$$

20   where $\rho_f = [(2n\times t_f\times w_f)/(b_w\times s_f)]$ is the FRP ratio for spaced FRP sheets while $\rho_f = (2n\times t_f/b_w)$

21   is for continuous FRP sheets; n, t_f (mm) and w_f (mm) are the number of FRP layers, the

22   thickness and the width of FRP sheets, respectively; E_f (N/mm^2) is the elastic modulus of

23   FRP; b_w (mm) is the width of the beam web; d_f (mm) is the effective height of FRP sheets; β

1 is the angle of FRP sheets and the longitudinal axis of beam; and s_f is the spacing of FRP

2 sheets;

3 In Eq. 20, the effective strain of FRP sheets, ε_{fe}, is obtained as follows:

4 $$\varepsilon_{fe} = \kappa_v \varepsilon_{fu} \leq 0.004 \tag{21}$$

5 where κ_v is the bonding factor and it is equal to $=[(k_1 k_1 L_e)/(11900\varepsilon_{fu})]$; $k_1 = (f_c'/27)^{2/3}$; $k_2 = [(d_f$

6 $- L_e)/d_f$]; L_e (mm) is the active bond length of FRP sheets, $=23300/(n \times t_f \times E_f)^{0.58}$; and ε_{fu} is the

7 rupture strain of FRP sheets.

8 <mark>As was mentioned above, although the stirrup strains were markedly lower in the</mark>

9 <mark>strengthened UPC beams than those in control ones, they far exceeded the yield strain at</mark>

10 <mark>beams failure. Therefore, the shear force of stirrups, V_{sw} (N), was estimated as follows:</mark>

11 $$V_{sw} = A_{sw} f_{yw} \frac{d_s}{s} = \rho_{sw} f_{yw} b_w d_s \tag{22}$$

12 The angle of the shear cracks of tested beams was observed from the test and varied from

13 25.6 to 40.3° (**Table 3**). Assuming that the angle is equal to 40° for the conservative purpose,

14 substituting Eqs. 6, 14–18, 20, and 22 into Eq. 2, and using MatLab Version 2015, the

15 reaction V_{re} can be approximated in the following form (with variation of ±4.5%):

16 $$V_{re} = \frac{0.085}{\sqrt[4]{d_e/1000}} \Omega \left(\frac{d_e}{a}\right)^{0.6} (f_c')^{0.33} (\rho_s)^{0.2} (1+0.2f_{pc}) \left[4.5(v_s + v_F) + 35\right](1+0.1v_P) b_w d_e \tag{23}$$

17 <mark>The influence of span-to depth ratio on shear resistance was quantified by the term</mark>

18 <mark>$1.6(d_e/a)^{0.6}$ in Eq. 23., which was established according to regression analysis (**Fig. 14**):</mark>

19 In Eq. 23, the coefficient Ω is given by:

20 $$\Omega = 10(d_p/L)^{0.35}/[(L/d_s - 1)] \tag{24}$$

21 The shear capacity of the beam, $V_u = V_{re}$ (N), is finally calculated as follows:

22 $$V_u = \frac{0.085}{\sqrt[4]{d_e/1000}} \Omega \left(\frac{d_e}{a}\right)^{0.6} (f_c')^{0.33} (\rho_s)^{0.2} (1+0.2f_{pc}) \left[4.5(v_{sw} + v_F) + 35\right](1+0.1v_P) b_w d_e \tag{25}$$

1   where $v_{sw} = V_{sw} / (b_w \times d_e)$; $v_F = V_F / (b_w \times d_e)$; and $v_P = V_P / (b_w \times d_e)$; d_e (mm) is the effective

2   depth of PC beams, $= [(A_p \times f_{py} \times d_p + A_s \times f_y \times d_s) / (A_p \times f_{py} + A_s \times f_y)]$; for V_{sw} see Eq. (22); for V_F

3   see Eq. (20); $V_p = F_p \sin\theta$ see Eq. (4). For other symbols used in Eq. (25) see the list of

4   symbols.

5   *Evaluation of the proposal formula*

6   The proposed model was verified against the experimental results of 57 beams including 22

7   beams in this study and 35 beams in the literature (Murphy et al. 2012; Kang and Ary, 2012;

8   Rupf et al. 2013, Herbrand and Classen, 2015, Nguyen et al. 2015, 2016; Qi et al. 2016).

9   Among these beams, there are 30 strengthened beams (19 post-tensioned beams and 11 pre-

10   tensioned beams) and 27 unstrengthened beams (24 post-tensioned beams and 3 pre-

11   tensioned beams). The investigated factors include: the concrete strength (from 28.3 MPa to

12   65.3 MPa), type of FRP (CFRP and GFRP), strengthening scheme (spaced U-wraps,

13   continuous U-wraps, and full-wrap), the FRP ratio ρ_f (from 0.06 % to 2.3%), the shear span

14   ratio a/d_e (from 1.53 to 7.96), the effective height of beams (from 283 mm to 1083 mm), the

15   trajectory of tendon (straight and harped), and the beam section (T, I, and rectangular). The

16   mean value (Mean = 1.02) and coefficient of variation (COV = 0.12) of the ratio $V_{u,theor}/V_{u,exp}$

17   summarized in **Table 4** demonstrate the proposed model is able to predict accurately the

18   shear resistance of the beams with a low variation. Particularly, the predictions of the

19   strengthened beams yield better performance with Mean =0.99 and COV =0.11 while the

20   corresponding numbers of the unstrengthened beams are Mean =1.04 and COV =0.13. The

21   predictions of the proposed model versus the experimental results are presented in **Fig. 15**. In

22   **Fig. 16**, the variation between $V_{u,theor}$ and $V_{u,exp}$ is examined against individual factors

23   including: the compressive strength of concrete f_c'; the effective concrete prestress f_{pc}; the

24   effective depth of beam d_e; the shear span to effective depth ratio a/d_e; the prestressing steel

25   ratio ρ_p; and the FRP shear reinforcement ratio ρ_f. Small variations of the ratio $V_{u,theor}/V_{u,exp}$

21

1   regarding the six factors show the high reliability of the proposed model.

2   *Comparison of the proposed design formula and design formulas given in codes*

3   Based on the experimental results of the PC beams (**Table 4**) and using the evaluation

4   procedure suggested by EC0 (1990), a shear design resistance model is proposed in which a

5   safety factor of 0.78 is taken into consideration. Moreover, to consider the difference between

6   cast-in-situ-concrete and concrete cast in labs, the proposed model also takes another factor

7   =1/1.15 (EC 2, 2004) into account. Finally, the final considered safety factor is 0.68

8   (=0.78/1.15), the design value of the shear resistance, $V_{u,d,prop}$, can be estimated as follows:

9    $$V_{u,d,prop} = \frac{0.058}{\sqrt[4]{d_e/1000}} \Omega \left(\frac{d_e}{a}\right)^{0.6} (f_c')^{0.33} (\rho_s)^{0.2} (1+0.2 f_{pc}) \left[4.5(v_s + v_F) + 35\right](1+0.1 v_P) b_w d_e \quad (26)$$

10   The shear resistances estimated by Eq. 26 were compared to that calculated according to ACI

11   440.2R (2008) and CNR DT200R1 (2013). The mean value and the coefficient of variation of

12   the ratio between the design shear resistances and the corresponding experimental values

13   ($V_{u,d}/V_{u,exp}$) were summarized in **Table 5** and **Fig. 17**. In general, all the design shear

14   resistances are conservative as compared to the experimental results and they can be used

15   safely for the design purpose. The models presented by ACI 440.2R (2008) and CNR-

16   DT200R1 (2013) yield quite similar results which are very conservative with Mean =0.49

17   and COV =0.34 for ACI 440.2R (2008) and Mean =0.48 and COV =0.31 for CNR-DT200R1

18   (2013). Among them, the proposed model shows a better mean value and smaller COV

19   (Mean =0.69, COV =0.12). While the models in the codes become more conservative when

20   the shear resistances of beams are greater than 500 kN, the proposed model yield more stable

21   variation as shown in **Fig. 18**.

22

1   *Contribution of concrete strength, prestressing force and FRP shear reinforcement to*

2   *shear resistance*

3   The contributions of concrete V_c (Eq. 19), the vertical component of tendons $V_p = F_p sin\theta$ (Eq.

4   19), the contribution of FRP sheets V_F (Eq. 20), and the contribution of stirrups V_{sw} (Eq. 22)

5   to the total shear resistance of the tested beams, $V_{u,theor}$, were summarized in **Table 6**. For the

6   strengthened beams, the contribution of concrete to the total shear resistance is dominant for

7   both the unbonded and bonded tendons. The average contributions of stirrups and FRP sheets

8   are 16% and 25%, respectively, which shows a very good agreement between the calculated

9   contribution of FRP sheets and the test results from this study. It is noted that the tested

10   beams in this study had straight tendons so that the contribution of the vertical component of

11   the tendons to the total shear resistance cannot be examined. It is necessary to conduct further

12   studies with non-straight tendons in order to be able to examine the contribution of this

13   component. For unstrengthened beams, the average contribution of concrete to the total shear

14   resistance is 50.4% for non-straight tendons and 76.8% for straight tendons for both the

15   unbonded and bonded tendons while the average contribution of stirrups is 22%. The average

16   contribution of the vertical component of the tendons to the total shear resistance is 22.8% for

17   unbonded tendons and 31.7% for bonded tendons, which agree well with the results of the

18   study by Qui et al. (2016).

19   **SUMMARY AND CONCLUSIONS**

20   This study investigates the shear behaviour of UPC beams strengthened with CFRP/GFRP U-

21   wraps and proposes a new model to predict the shear resistance of PC beams strengthened

22   with FRP. The findings in this study can be summarized as follows:

23   1. The FRP type does not significantly affect the efficiency of shear strengthening UPC

24   beams. Although the stiffness of the CFRP sheets was 2.8 times higher than that of

25   GFRP sheets, the shear resistance of the CFRP strengthened beams was just

proximately 5% greater than that of the GFRP strengthened beams. The enhancement efficiency of GFRP/CFRP U-wraps increases with the concrete strength. Using CFRP/GFRP U-wraps for the shear strengthening increases the shear-cracking load up to 40%, the shear resistance up to 29%, reduces the crack development rate and stiffness degradation rate while improving the ductility and the deformation capacity of the beams up to 1.7 times.

2. Reduction of the shear span to effective depth ratio increased the shear resistance of the beams and simultaneously reduced the strain of FRP sheets. Reducing this ratio from 2.3 to 1.5 led to an average increase of the shear resistance by 27% and a reduction of the maximum strain of FRP sheets up to 29%. The reason is that the reduction of the ratio leads to an increase of the inclined crack angle and thus reduces the angle between FRP sheets and the cracks. As a result, the contribution of FRP sheets to the total shear resistance and strain of FRP sheets becomes smaller. In addition, the smaller the shear span to effective depth ratio, the more-like arch analogy beams, leading to a lower efficiency of FRP sheets.

3. The maximum strain of FRP sheets increased with the concrete strength. The spaced GFRP/CFRP U-wraps had the maximum strain much greater than that of the continuous ones. The stress concentration caused these variations which were about 2 – 2.3 times for CFRP and 1.3 – 1.5 times for GFRP, respectively. The maximum strain of CFRP sheets was 3.6‰ for continuous U-wraps and 7.2‰ for spaced U-wraps, which correspond to approximately 36% and 72% of the rupture strain of CFRP sheets, respectively; while the maximum strain of GFRP sheets was 5.5‰ for continuous U-wraps and 8.5‰ for spaced U-wraps, which correspond to approximately 25% and 39% of the rupture strain of GFRP sheets, respectively. These values show that the limit strain = 4‰ according to ACI 440.2R (2008) is much

24

conservative, which should be adjusted particularly for spaced GFRP U-wraps in order to ensure economic aspect of the design.

4. In the shear span region, the tendons and the longitudinal reinforcements did not yield. The maximum strain of the tendons and the longitudinal reinforcements in the shear span region was 7.8‰ and 2‰, corresponding to 91% and 93% of their yield strain, respectively. This finding indicates that the assumption that tendons and longitudinal reinforcement yield at the ultimate stage may not reflect the actual behaviour of UPC beams. This assumption may lead to an unconservative prediction of the shear resistance of UPC beams. Because of the stress concentration, the maximum strain of concrete at the loading points was from 2.8‰ to 3.4‰, which was average 2.7 times greater than that at the midspan.

5. The theoretical proposed model shows very close predictions to the experimental results and stable variation for both strengthened beams and unstrengthened beams, evident by the mean value of the ratio $V_{u,theor}/V_{u,exp}$ and the coefficient of variation (COV) of 1.02 and 0.12, respectively.

6. The design shear strength models in ACI 440.2R (2008) and CNR-DT 200 R1 (2013) yield very conservative predictions, resulting in very high safety factors while the design proposed model shows a little bit smaller safety factor and lower variation so that the proposed model can be used safely with higher reliability.

7. Because of the lack of the experimental results, there is a need for further studies to properly evaluate the efficiency of using FRP U-wraps to strengthen UPC beams. In the future, studies about anchorage systems for U-wraps and non-straight tendons are sought.

4 **REFERENCES**

5 ACI Committee 318, 2014. *Building Code Requirements for Structural Concrete (ACI 318-14)*,

6   Farmington Hills, MI: American Concrete Institute (ACI).

7 ACI Committee 440, 2008. *Guide for the Design and Construction of Externally Bonded FRP*

8   *Systems (ACI 440.2R-08)*, Farmington Hills, MI: American Concrete Institute (ACI).

9 Advisory committee on Technical recommendations for construction, 2013. *Guide for the Design and*

10   *Construction of externally bonded FRP systems for strengthening existing structures (CNR-DT*

11   *200 R1/2013)*, Rome.

12 Al-Rousan, R.Z. and Issa, M. A., 2016. The effect of beam depth on the shear behavior of reinforced

13   concrete beams externally strengthened with cacbon fiber-reinforced polymer composites.

14   *Advances in Structural Engineering*, *19*(11), pp.1769-1779.

15 Ary, M.I. and Kang, T.H.K., 2012. Shear-strengthening of reinforced & prestressed concrete beams

16   using FRP: Part I-Review of previous research. *International Journal of Concrete Structures*

17   *and Materials*, *6*(1), pp.41-47.

18 Belarbi, A., Bae, S.W., Ayoub, A., Kuchma, D., Mirmiran, A., Okeil, A. and Hanna, N., 2011. *Design*

19   *of FRP Systerms for strengthening concrete girders in shear (NCHRP Report 678)*, Washington

20   DC (USA): Transportation Research Board.

21 Bousselham, A., and Chaallal, O., 2004. Shear strengthening reinforced concrete beams with fiber-

22   reinforced polymer: Assessment of influencing parameters and required research. *ACI*

23   *Structural Journal*, *101*(2), pp.219–227.

24 Bousselham, A., and Chaallal, O., 2006. Effect of transverse steel and shear span on the performance

25   of RC beams strengthened in shear with CFRP. *Composites Part B*, *37*(1), pp.37–46.

26 British Standards Institution, 2002. *Eurocode - Basic of Structural design (EN 1990)*. British

27   Standards Institution.

1   British Standards Institution, 2004. *Eurocode 2: Design of Concrete Structures: Part 1-1: General*

2   *Rules and Rules for Buildings (EN 1992-1-1)*. British Standards Institution.

3   Chajes, M.J., Finch Jr., W.W., Januszka, T.F., and Thomson Jr., T.A., 1996. Bond and force transfer

4   of composite material plates bonded to concrete. *ACI Structural Journal*, *93*(2), pp.209-217.

5   Chen, G.M, Zhang, Z., Li, Y.L., Li, X.Q., Zhou, C.Y., 2016. T-section RC beams shear-

6   strengthened with anchored CFRP U-strips. *Composite Structures*, *144*, pp.57-79.

7   Chen G.M., Teng J.G., Chen J.F., Rosenboom O.A. (2010) "Interaction between Steel Stirrups and

8   Shear-Strengthening FRP Strips in RC Beams", Journal of Composites for Construction, 14(5),

9   pp. 498-509.

10   Chen, G.M., Teng, J.G. and Chen, J.F., 2012. Process of debonding in RC beams shear-strengthened

11   with FRP U-strips or side strips. *International Journal of Solids and Structures*, *49*(10),

12   pp.1266-1282.

13   Chen G.M., Teng J.G., Chen J.F. (2013) "Shear Strength Model for FRP-Strengthened RC Beams

14   with Adverse FRP-Steel Interaction", Journal of Composites for Construction, 17(1), pp. 50-66.

15   Colotti, V., 2016. Effectiveness factors for bond strength in FRP shear-strengthened RC

16   beams. *Materials and Structures*, *49*(12), pp.5031-5049.

17   Concrete Society Commitee, 2012. *Design Guidance for Strengthening Concrete Structures using*

18   *Fibre Composite Materrials (Technical Report No. 55) 3rd ed.*, Camberley, Surrey.

19   Deniaud, C. and Cheng, J.R., 2001. Shear behavior of reinforced concrete T-beams with externally

20   bonded fiber-reinforced polymer sheets. *ACI Structural Journal*, *98*(3), pp.386-394.

21   Dias, S.J.E., and Barros, J.A.O., 2013. Shear strengthening of RC beams with NSM CFRP laminates:

22   experimental research and analytical formulation. *Composite Structures, 99*, pp.477–490.

23   Dror, E.B. and Rabinovitch, O., 2016. Size effect in the debonding failure of FRP strengthened

24   beams. *Engineering Fracture Mechanics*, *156*, pp.161-181.

25   Guo, Z.G., Cao, S.Y., Sun, W.M. and Lin, X.Y., 2005, December. Experimental study on bond stress-

26   slip behaviour between FRP sheets and concrete. In *FRP in construction, proceedings of the*

27   *international symposium on bond behaviour of FRP in structures* (pp. 77-84).

1   Herbrand, M. and Classen, M., 2015. Shear tests on continuous prestressed concrete beams with

2   external prestressing. *Structural Concrete*, *16*(3), pp.428-437.

3   Hognestad, E., 1951. *Study of combined bending and axial load in reinforced concrete members*.

4   University of Illinois at Urbana Champaign, College of Engineering. Engineering Experiment

5   Station.

6   Hutchinson, R., Donald, D., Abdelrahman, A., and Kizkalla, S., 1998. Shear

7   strengthening of prestressed concrete bridge girders using bonded CFRP sheets. *ECCM-8*, *2*,

8   pp.43-50.

9   Kang, T.H.K. and Ary, M.I., 2012. Shear-strengthening of reinforced & prestressed concrete beams

10   using FRP: Part II—Experimental investigation. *International Journal of Concrete Structures*

11   *and Materials*, *6*(1), pp.49-57.

12   Khalifa, A. and Nanni, A., 2000. Improving shear capacity of existing RC T-section beams using

13   CFRP composites. *Cement and Concrete Composites, 22*(3), pp.165-174.

14   Kim, Y., Quinn, K., Satrom, N., Garcia, J., Sun, W., Ghannoum, W.M. and Jirsa, J.O., 2012. *Shear*

15   *strengthening of reinforced and prestressed concrete beams using carbon fiber reinforced*

16   *polymer (CFRP) sheets and anchors*. Technical Rep. No. FHWA/TX-12/0-6306-1, Center for

17   Transportation Research, University of Texas at Austin, Austin, Texas.

18   Li, W. and Leung, C.K., 2015. Shear span–depth ratio effect on behavior of RC beam shear

19   strengthened with full-wrapping FRP strip. *Journal of Composites for Construction*, *20*(3),

20   pp.1-14.

21   Li, W. and Leung, C.K., 2017. Effect of shear span-depth ratio on mechanical performance of RC

22   beams strengthened in shear with U-wrapping FRP strips. *Composite Structures* (in press).

23   https://doi.org/10.1016/j.compstruct.2017.06.059

24   Mostofinejad, D., Hosseini, S.A. and Razavi, S.B., 2016. Influence of different bonding and wrapping

25   techniques on performance of beams strengthened in shear using CFRP

26   reinforcement. *Construction and Building Materials*, *116*, pp.310-320.

27   Murphy, M., Belarbi, A. and Bae, S.W., 2012. Behavior of prestressed concrete I-girders strengthened

28   in shear with externally bonded fiber-reinforced-polymer sheets. *PCI journal*, *57*(3), pp.63-82.

Nguyen, T.T.D., Matsumoto, K., Sato, Y., Yamada, M. and Niwa, J., 2016. Shear-resisting mechanisms of pre-tensioned PC beams without shear reinforcement strengthened by CFRP sheets. *Journal of JSCE*, *4*(1), pp.59-71.

Nguyen, T.T.D., Matsumoto, K., Yamada, M. And Niwa, M., 2015. Behaviors of pretensioned PC beams strengthened in shear using externally bonded CFRP sheets. *JCI Concrete Journal, 37*(2), pp.1183-1188.

Nguyen-Minh, L. and Rovňák, M., 2015. Size effect in uncracked and pre-cracked reinforced concrete beams shear-strengthened with composite jackets. *Composites Part B*, *78*, pp.361-376.

Pellegrino, C. and Modena, C., 2006. Fiber-reinforced polymer shear strengthening of reinforced concrete beams: Experimental study and analytical modeling. *ACI Structural Journal*, *103*(5), pp.720-728.

Pellegrino C., Modena C. (2008). "An experimentally based analytical model for shear capacity of FRP strengthened reinforced concrete beams", Mechanics of Composite Materials, 44(3), pp. 231-244.

Pellegrino C., Vasic M. (2013). "Assessment of design procedures for the use of externally bonded FRP composites in shear strengthening of reinforced concrete beams", Composites Part B: Engineering, 45(1), pp. 727-741.

Perera, R., Arteaga, A., and Diego, D.A., 2010. Artificial intelligence techniques for prediction of the capacity of RC beams strengthened in shear with external FRP reinforcement. *Composite Structures*, *92*(5), pp.1169-1175.

Qi, J.N., Wang, J.Q., Ma, Z.J. and Tong, T., 2016. Shear behavior of externally prestressed concrete beams with draped tendons. *ACI Structural Journal*, *113*(4), pp.677-688.

Reed, C.E. and Peterman, R.J., 2004. Evaluation of prestressed concrete girders strengthened with carbon fiber reinforced polymer sheets. *Journal of Bridge Engineering*, *9*(2), pp.185-192.

Rupf, M., Ruiz, M.F. and Muttoni, A., 2013. Post-tensioned girders with low amounts of shear reinforcement: Shear strength and influence of flanges. *Engineering Structures*, *56*, pp.357-371.

Tam, A. and Pannell, F.N., 1976. The ultimate moment of resistance of unbonded partially prestressed reinforced concrete beams. *Magazine of Concrete Research*, *28*(97), pp.203-208.
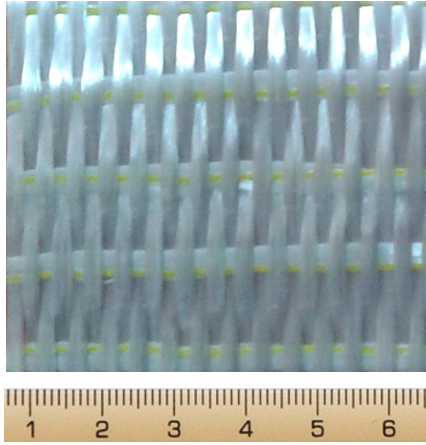
<div align="center">(a)   (b)</div>
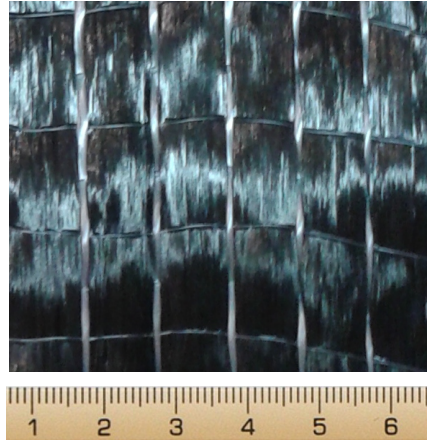
Fig. 1: Unidirectional fabrics with: (a) glass fibres; (b) carbon fibres

Fig. 2: Details of the tested beams: (a) arrangement of tendons, stirrups and strain gauges; (b) beam section

Fig. 3: Test setup: (a) beams with CFRP material; (b) beams with GFRP material;
(c) beams strengthened by spaced FRP U-wraps; (d) beams strengthened by continuous FRP U-wraps
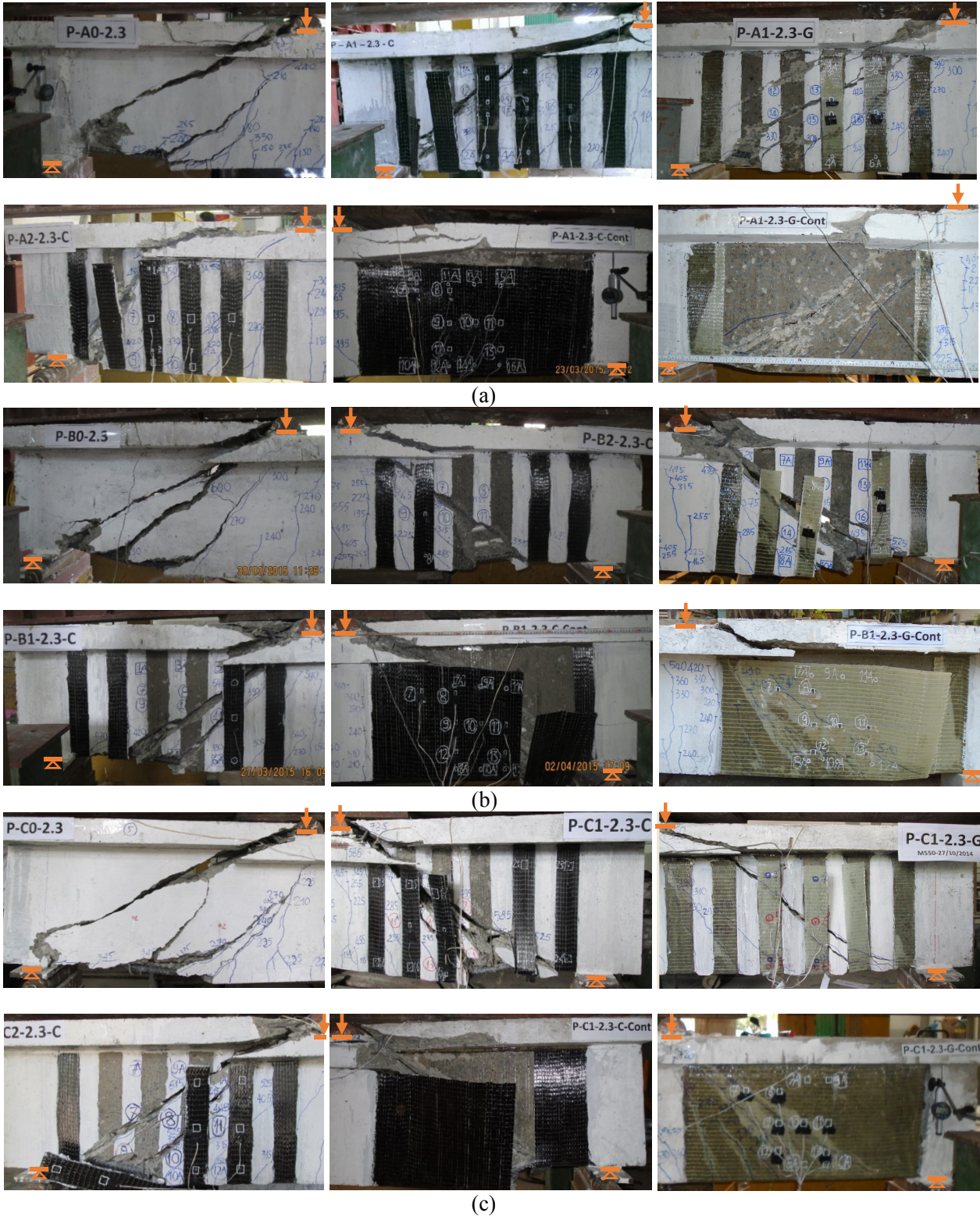
Fig. 4: Typical failure pattern of tested beams: (a) group A; (b) group B; and (c) group C

Fig. 5: Relative load – displacement of tested beams: (a) group A; (b) group B; and (c) group C
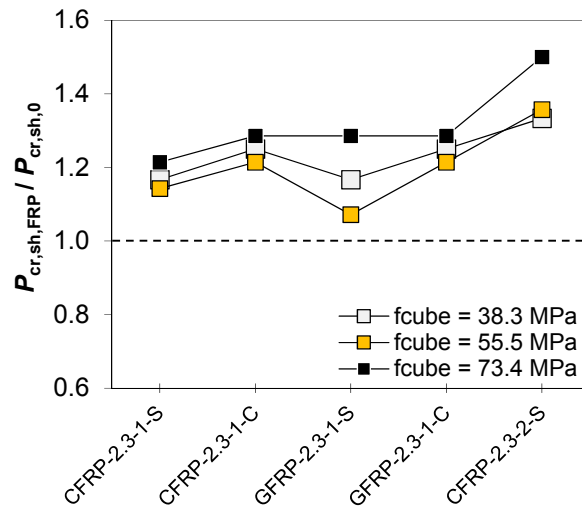
Note: the first character states the type of FRP (CFRP or GFRP), the second one indicates the ratio a/d_e (1.5, 1.9, and 2.3), the third character states the number of FRP layers (1 or 2), the last character represents the strengthening scheme (S – strips with spacing, C – continuous strips)

Fig. 6: Comparison of shear-cracking force of the FRP strengthened beams versus the control beams

(a)   (b)
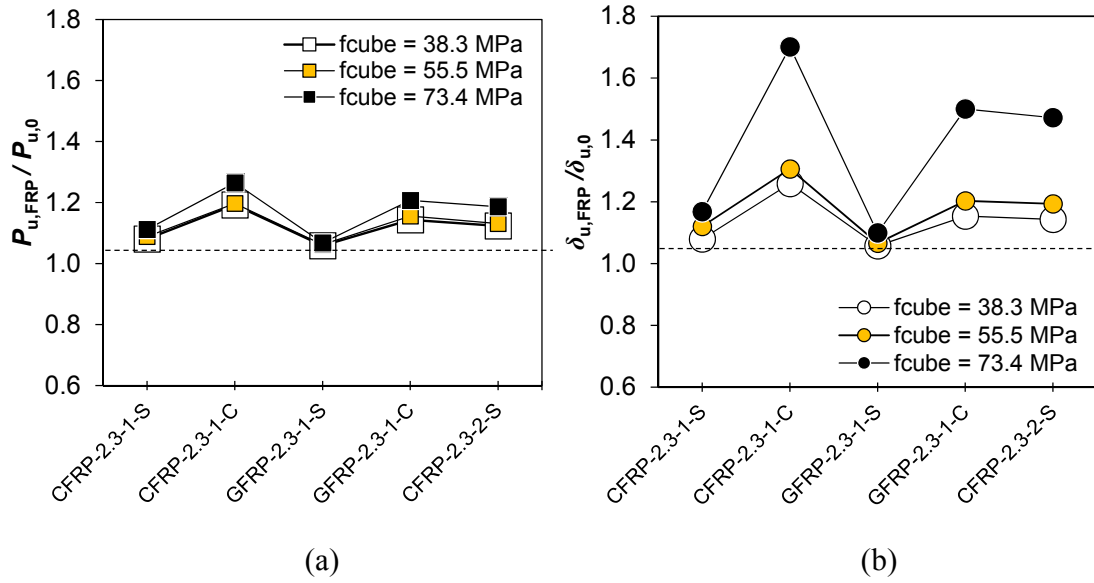
Note: the first character states the type of FRP (CFRP or GFRP), the second one indicates the ratio a/d_e (1.5, 1.9, and 2.3), the third character states the number of FRP layers (1 or 2), the last character represents the strengthening scheme (S – spaced U-wraps, C – continuous U-wraps)

Fig. 7: Comparison of FRP strengthened beams and control beams: (a) maximum load; and (b) total deflection
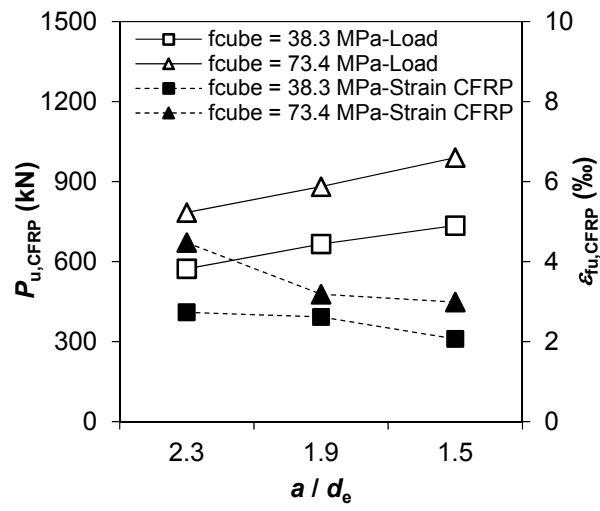
Fig. 8: Maximum load of FRP-strengthened beams and maximum strain of CFRP sheets versus ratio a/d_e
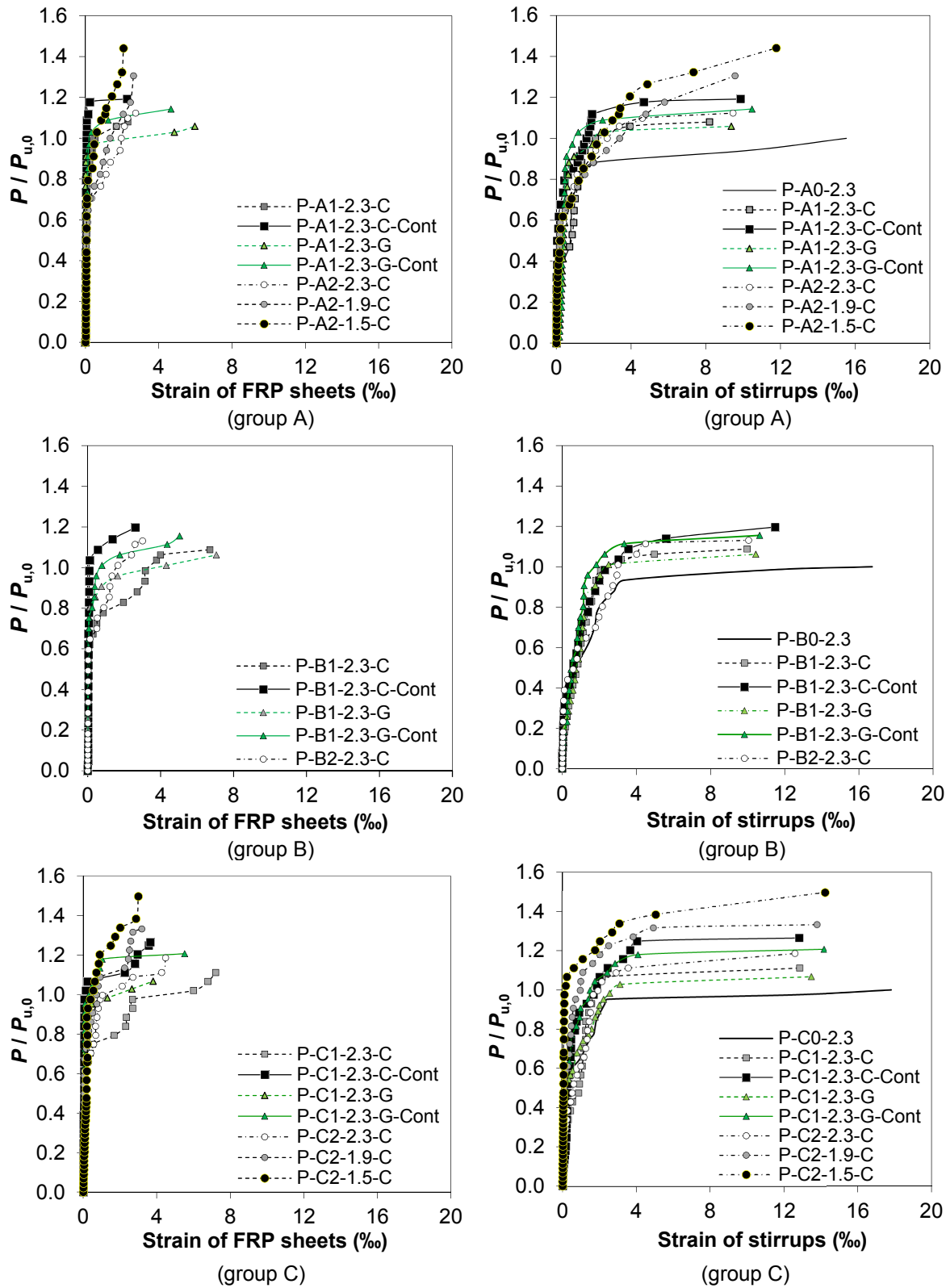
Fig. 9: Load-strain relationship of FRP sheets and stirrups of tested beams
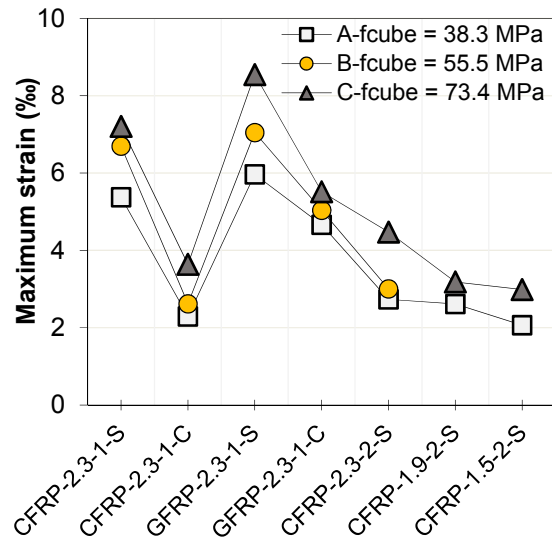
Note: the first character states the type of FRP(CFRP or GFRP), the second one indicates the ratio a/d_e (1.5, 1.9, and 2.3), the third character states the number of FRP layers (1 or 2), the last character represents the strengthening scheme (S – strips with spacing, C – continuous strips)

Fig. 10: Maximum strain of FRP sheets of the tested beams
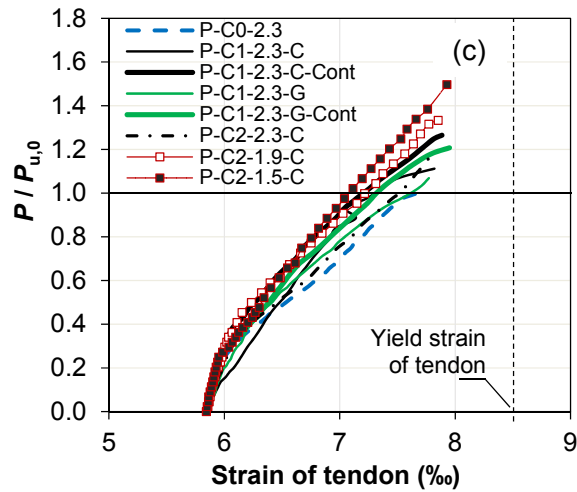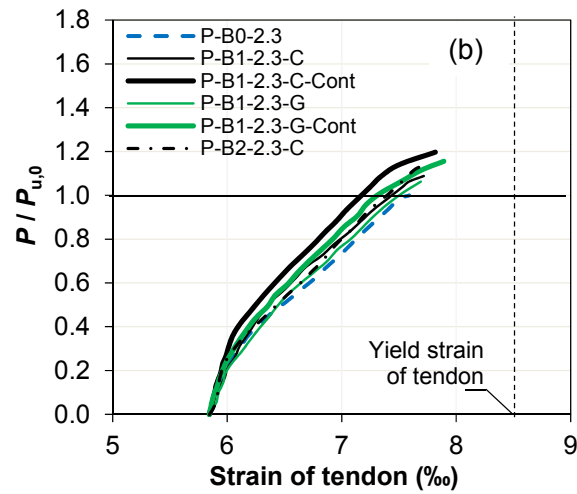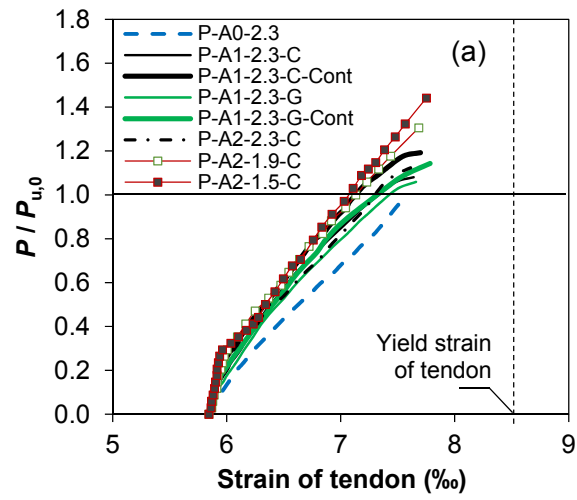
Fig. 11: Relative load-strain of tendons at midspan: (a) group A; (b) group B; and (c) group C
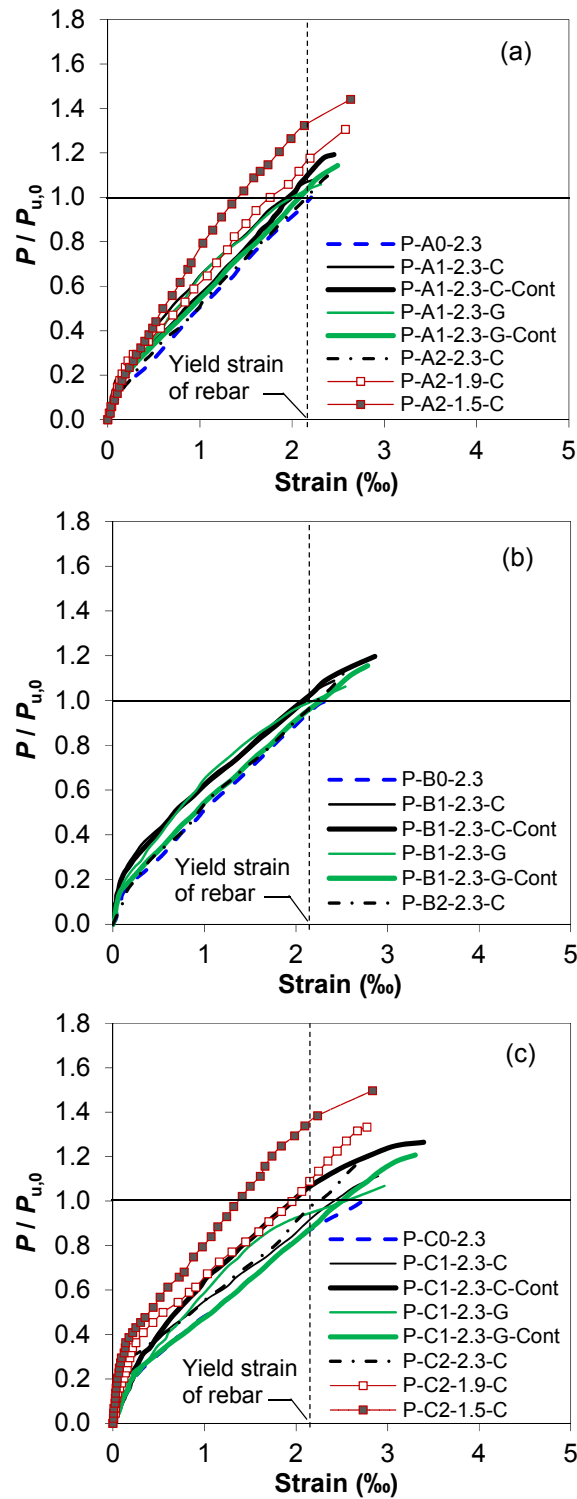
Fig. 12: Relative load-strain in rebars at midspan: (a) group A; (b) group B; and (c) group C
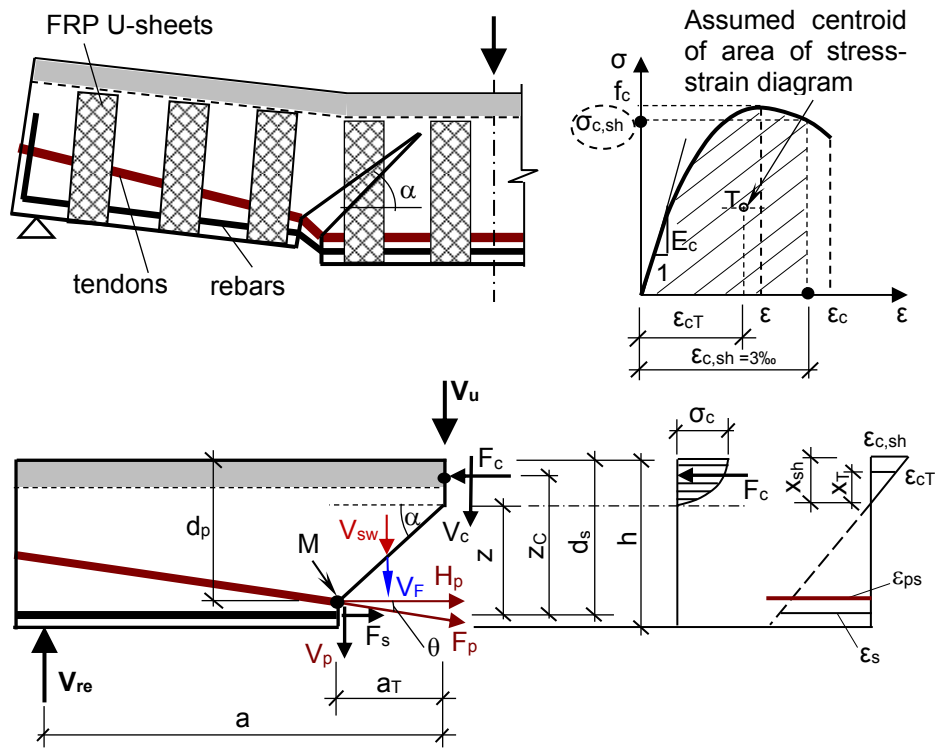
Fig. 13: Free body diagram of a simply supported beam and assumptions for shear crack
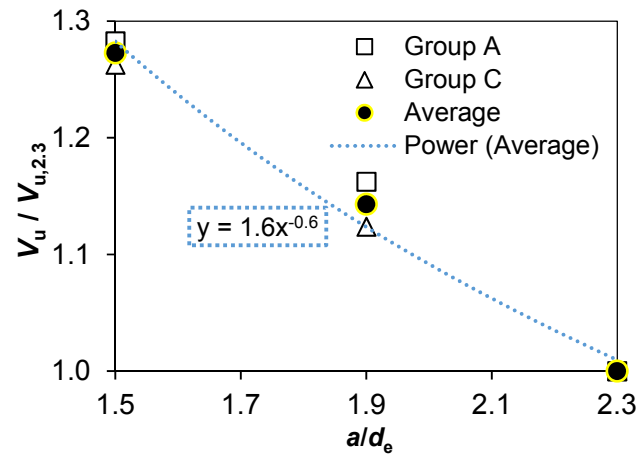
Note: $V_{u,2.3}$ is the shear resistance of the CFRP strengthened beams with the ratio $a/d_e = 2.3$.

Figure 14: Influence of the ratio a/d_e to the shear resistance V_u
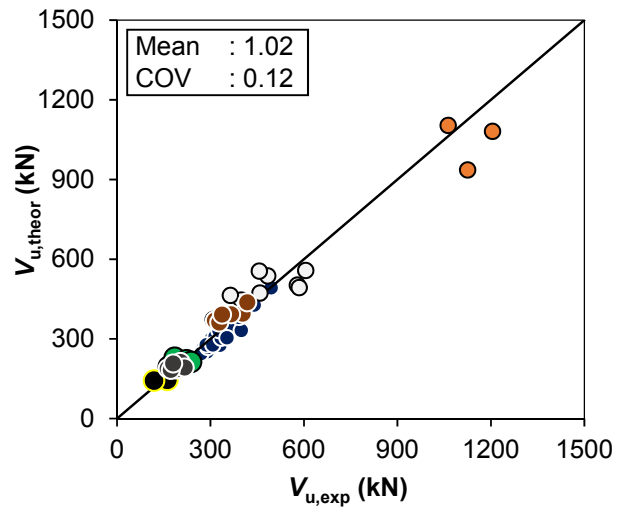
Fig. 15: Comparison between predicted and experimental shear capacities
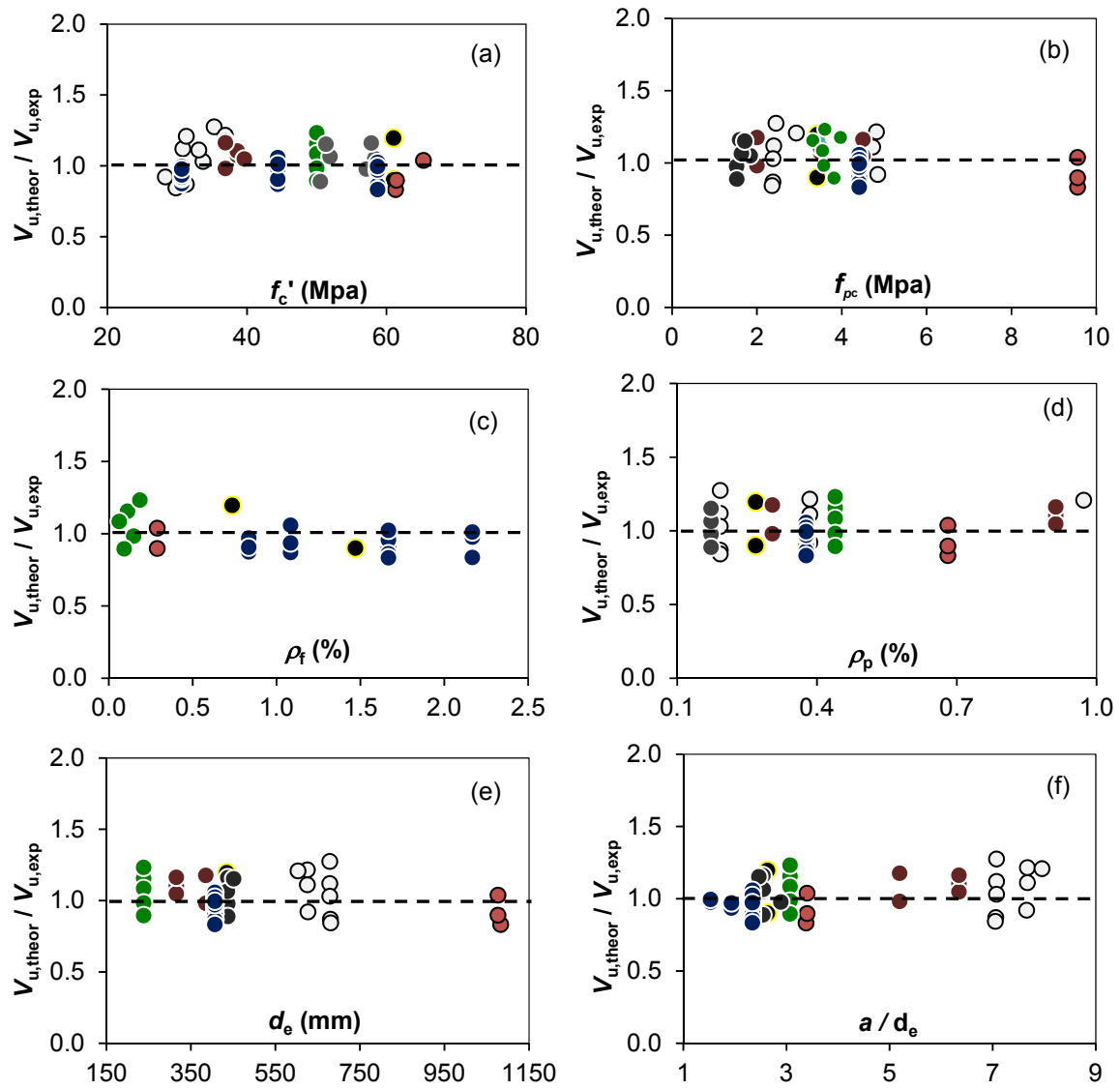
Fig. 16: Evaluation of proposed formula for various parameters: (a) f_c'; (b) f_{pc}; (c) ρ_f ; (d) ρ_p; (e) d_e; and (f) a/d_e
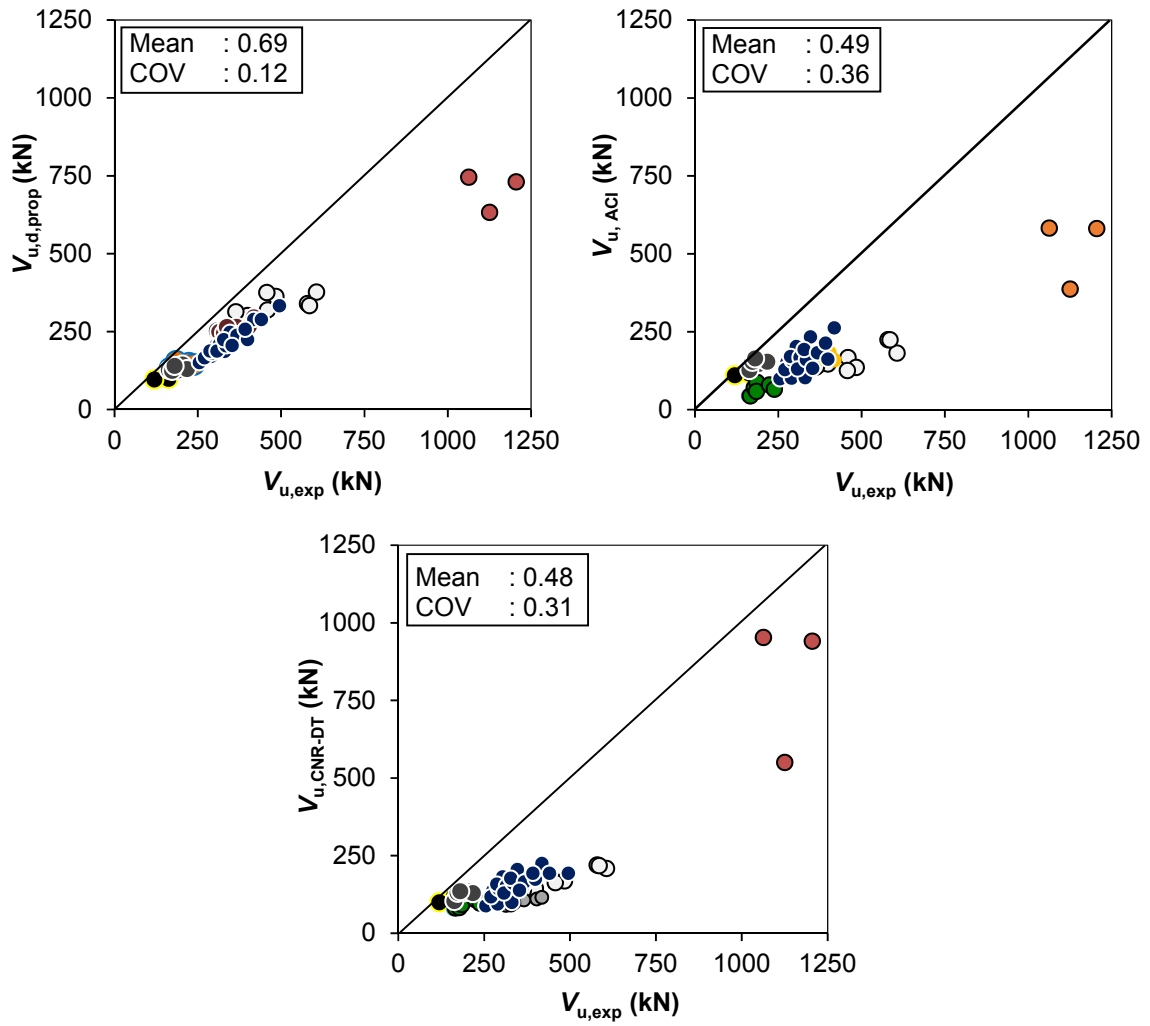
Fig. 17: Comparison of design and experimental shear resistances
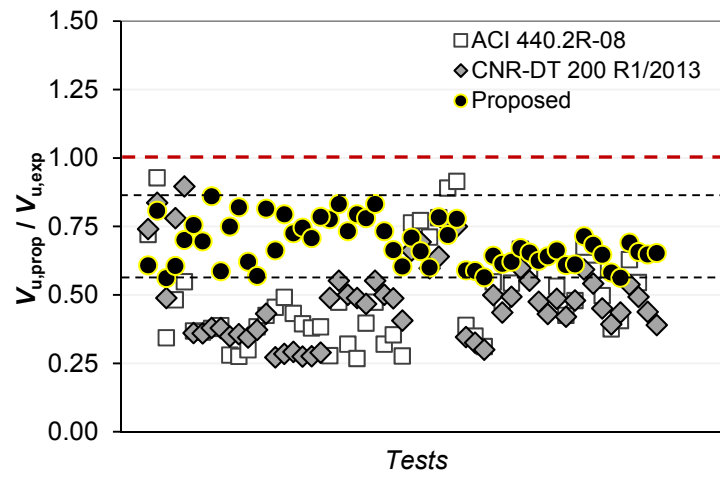
Fig. 18: Comparison of design to experimental shear resistance ratio

LIST OF FIGURES
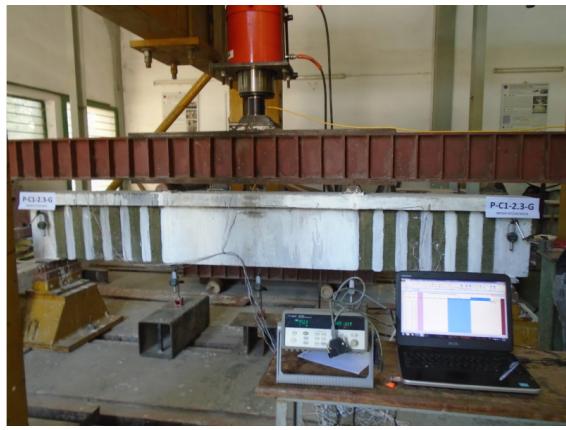
Fig. 1: Unidirectional fabrics with: (a) glass fibres; (b) carbon fibres

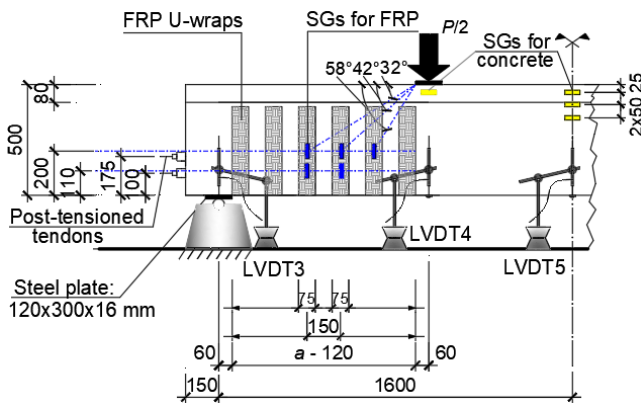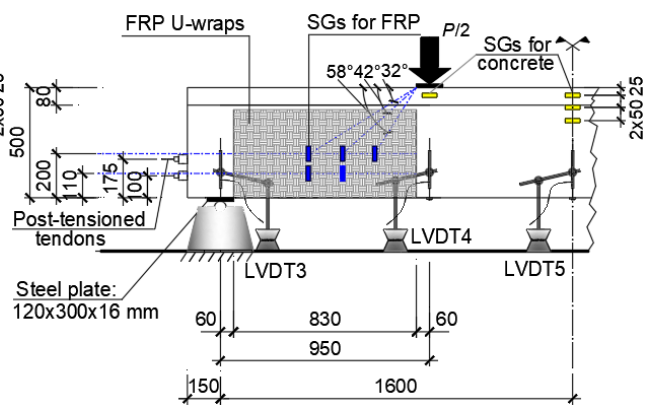**Fig. 2**: Details of the tested beams: (a) arrangement of tendons, stirrups and strain gauges; (b) beam section

Fig. 3: Test setup: (a) beams with CFRP material; (b) beams with GFRP material; (c) beams strengthened by spaced FRP U-wraps; (d) beams strengthened by continuous FRP U-wraps

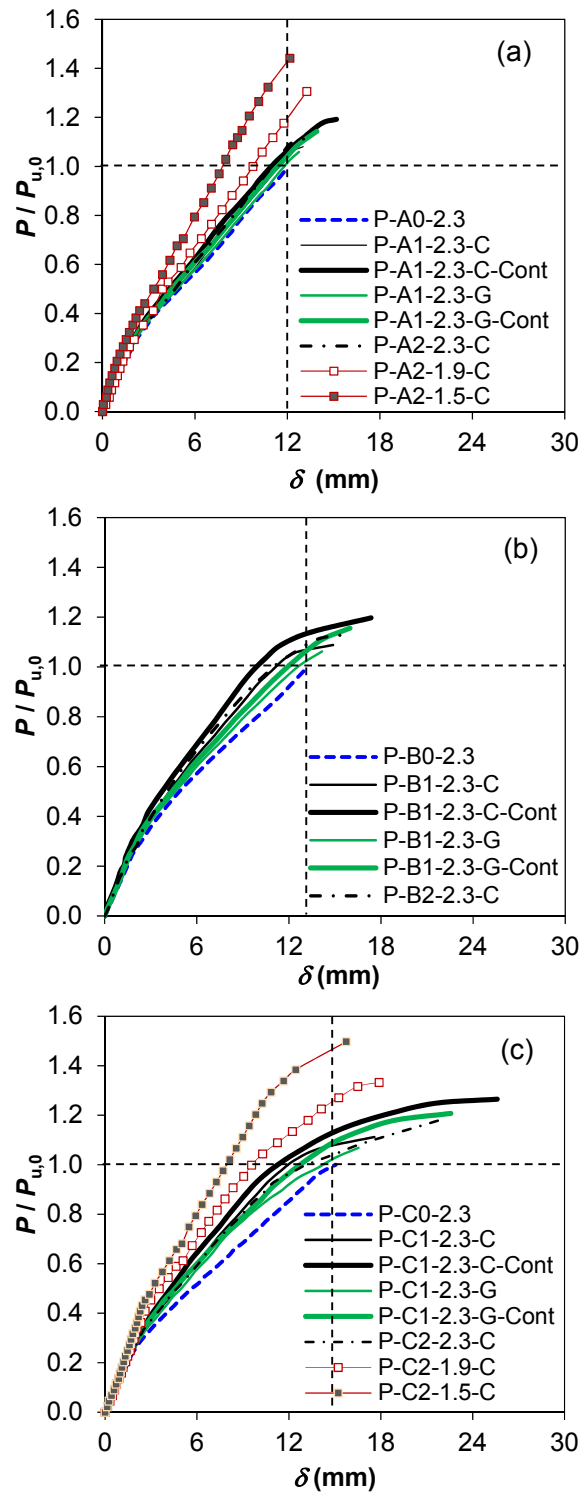**Fig. 4**: Typical failure pattern of the tested beams: (a) group A; (b) group B; and (c) group C

Fig. 5: Relative load – displacement of tested beams: (a) group A; (b) group B; and (c) group C

Fig. 6: Comparison of shear-cracking force of the FRP strengthened beams versus the control beams

Fig. 7: Comparison of FRP strengthened beams and control beams: (a) maximum load; and (b) total deflection

Fig. 8: Maximum load of FRP-strengthened beams and maximum strain of CFRP sheets versus ratio a/d_e

Fig. 9: Load-strain relationship of FRP sheets and stirrups of the tested beams

Fig. 10: Maximum strain of FRP sheets of the tested beams

Fig. 11: Relative load-strain of tendons at midspan: (a) group A; (b) group B; and (c) group C

Fig. 12: Relative load-strain in rebars at midspan: (a) group A; (b) group B; and (c) group C

Fig. 13: Free body diagram of a simply supported beam and assumptions for shear crack

Fig. 14: Influence of the ratio a/d_e to the shear resistance V_u

Fig. 15: Comparison between predicted and experimental shear capacities

Fig. 16: Evaluation of proposed formula for various parameters: (a) f_c'; (b) f_{pc}; (c) ρ_f; (d) ρ_p; (e) d_e; and (f) a/d_e

Fig. 17: Comparison of design and experimental shear resistances

Fig. 18: Comparison of design to experimental shear resistance ratio

LIST OF SYMBOLS

a	: shear span of a beam, mm;
a_T	: horizontal projection of the diagonal crack length, mm;
b, b_w	: width of beam web, mm;
b_f	: width of beam flange, mm;
d, d_e	: effective depth of a beam, $= [(A_p \times f_{py} \times d_p + A_s \times f_y \times d_s)/(A_p \times f_{py} + A_s \times f_y)]$, mm;
d_p	: effective depth to prestressing tendons, mm;
d_f	: effective depth of FRP shear reinforcement, mm;
d_s	: effective depth to steel rebars, mm;
f_c	: mean compressive strength of concrete cylinders, N/mm^2;
f_c'	: nominal compressive strength of concrete cylinders, N/mm^2;
$f_{c,cube}, f_{cube}$	: mean compressive strength of concrete cubes, N/mm^2;
$f_{sp,cube}$	: mean splitting strength of concrete cubes, N/mm^2;
f_y	: yield strength of steel rebars, N/mm^2;
f_u, f_{uf}	: ultimate tensile strengths of steel rebars and FRP sheets, respectively, N/mm^2;
f_{yw}, f_{uw}	: yield and ultimate tensile strength of stirrups, respectively, N/mm^2;
f_{pc}	: effective prestress, $= \Sigma P/A_c$, N/mm^2;
f_{py}, f_{pu}	: yield and ultimate strength of tendons, N/mm^2;
f_t	: maximum concrete's tensile stress due to jacking force at prestress transfer stage, N/mm^2;
h	: overall depth of beam, mm;
h_f	: thickness of beam flange, mm;
k_1, k_2	: modification factors, $k_1 = (f_c'/27)^{2/3}$ and $k_2 = (d_f - L_e)/d_f$ according to ACI 440.2R (2008);
n	: number of FRP layers;
n_p	: number of tendons;
s	: stirrup spacing, mm;
s_f	: FRP U-wrap spacing, mm;
t_f	: total thickness of FRP sheets, mm;
w_f	: width of FRP sheets, mm;
x_{sh}	: depth of concrete compressive zone in shear, mm;
x_T	: distance from neutral axis to centroid of area under the stress–strain diagram, mm;
z	: vertical projection of diagonal crack length, mm;

z_c : lever arm of internal forces, mm;

A_c : cross-section area of beam, mm^2;

A_p : cross-section area of tendons, mm^2;

A_s : cross-section area of steel rebars, mm^2;

A_{sw} : cross-section area of steel stirrups, mm^2;

E_c : elasticity modulus of concrete, N/mm^2;

E_f, E_p, E_s : elasticity modulus of FRP sheets, tendons and tensile rebars, respectively, N/mm^2;

F : effective prestresing force in one tendon, N;

F_c : compressive force in concrete, N;

F_p : force in tendons, N;

F_{pi} : initial prestressing force in tendons, kN;

F_s : force in tensile rebars, N;

H_p : horizontal component of force in tendons, N;

L_0, L : length and span of beam, respectively, mm;

L_e : active bond length of FRP sheets, mm;

P : force, kN;

$P_{cr,fl}$: flexural cracking force, kN;

$P_{cr,sh}$: shear cracking force, kN;

$P_{cr,sh,FRP}$, $P_{cr,sh,0}$: shear cracking force of FRP strengthened beams and control beam, kN;

$P_{deb,CFRP}$, $P_{deb,GFRP}$: initial debonding force of CFRP / GFRP sheets, kN;

$P_{u,0}$: experimental maximum force of control beam, kN;

$P_{u,deb}$: initial debonding force of FRP sheets, kN;

$P_{u,CFRP}$, $P_{u,GFRP}$: maximum load of CFRP / GFRP-strengthened beam, kN;

$P_{u,FRP}$: maximum load of FRP-strengthened beam, kN;

$P_{u,tot,exp}$: experimental maximum force, kN;

V_c : contribution of concrete to shear resistance, N;

V_F : contribution of FRP sheets to shear resistance, N;

V_p : vertical component of tendon force, N;

V_{re} : reaction force, N;

V_u : shear resistance, N;

$V_{u,2.3}$: shear resistance of the CFRP strengthened beams with the ratio $a/d_e = 2.3$;

$V_{u,ACI}$	: design shear resistance calculated according to ACI 440.2R (2008), N;
$V_{u,CNR-DT}$	: design shear resistance calculated according to CNR DT 200R1 (2013), N;
$V_{u,d}$	: design shear resistance, N;
$V_{u,prop,d}$	: design resistance calculated according to proposed formula, N;
$V_{u,exp}$	: experimental shear resistance, N;
$V_{u,theor}$	: theoretical shear resistance of beam, N;
V_{sw}, V_s	: contribution of stirrups to shear resistance, N;
α	: angle of shear crack to longitudinal axis of beam, degree;
β	: angle of orientation of principal fibers to longitudinal axis of beam, degree;
θ	: angle of tendons to longitudinal axis of beam, degree;
Ω	: coefficient from Eq. (24);
σ	: stress, N/mm^2;
σ_c	: stress in concrete, N/mm^2;
$\sigma_{c,sh}$	: compressive stress in concrete at shear failure, N/mm^2;
ε	: strain, ‰;
ε_0	: compressive strain at peak stress, ‰;
ε_c	: strain in concrete, ‰;
$\varepsilon_{c,sh}$	: compressive strain in concrete at shear failure, ‰;
ε_{cT}	: compressive strain in concrete at the centroid of the area under the stress–strain diagram, ‰;
$\varepsilon_{cu,mid}$, $\varepsilon_{cu,pld}$	: compressive strain of concrete at midspan and loading point at beam failure, respectively, ‰;
ε_{fe}	: effective strain of FRP sheets, ‰;
$\varepsilon_{FRP,u}$	: maximum strain of FRP sheets at beam failure, ‰;
ε_{pe}	: effective pre-stressing strain of tendons, ‰;
ε_{ps}	: strain in tendons at beam failure, ‰;
$\varepsilon_{pu,mid}$, $\varepsilon_{pu,end}$	: strain in tendons at midspan and near the support at beam failure, respectively, ‰;
$\varepsilon_{su,mid}$, $\varepsilon_{su,end}$	: strain in rebars at midspan and near the support at beam failure, respectively, ‰;
ε_{fu}	: rupture strain of FRP sheets, ‰;
ε_{wu}	: stirrup strain at beam failure, ‰;
δ	: beam displacement at midspan, mm;

$\delta_{u,mid}$: beam deflection at midspan at failure, mm;

$\delta_{u,FRP}$, $\delta_{u,0}$: deflection of FRP strengthened beam and control beam at midspan at failure, respectively, mm;

κ_v : bond-reduction coefficient, $\kappa_v = (k_1 k_1 L_e)/(11900 \varepsilon_{fu})$ according to ACI 440.2R (2008)

ρ_f : FRP sheet ratio, %;

ρ_s : tensile longitudinal reinforcement ratio, %;

ρ_{sw} : shear reinforcement stirrups ratio, %;

ρ_p : prestressing steel ratio, %;

v_s : nominal shear strength (stress) provided by steel stirrups, $= V_s/(b_w d_e)$, N/mm^2;

v_F : nominal shear strength (stress) provided by FRP stirrups, $= V_F/(b_w d_e)$, N/mm^2;

v_p : shear strength (stress) provided by vertical component of prestressing force, $= V_p/(b_w d_e)$, N/mm^2.

LIST OF TABLES

Table 1a: Mechanical properties of concrete and tendons

Concrete						Tendon[a]		
Group A		Group B		Group C				
$f_{c,cube}$	$f_{sp,cube}$	$f_{c,cube}$	$f_{sp,cube}$	$f_{c,cube}$	$f_{sp,cube}$	f_{pu}	f_{py}	E_p
MPa	MPa	MPa	MPa	MPa	MPa	MPa	MPa	GPa
38.3	3.9	55.5	6.9	73.4	8.6	1860	1675	197

Table 1b: Mechanical properties of <mark>fiber fabric</mark> and steel reinforcements

Carbon fiber fabrics [a]			Glass fiber fabrics [a]			Longitudinal rebars			Stirrups	
f_{uf} MPa	E_f GPa	ε_{uf} %	f_{uf} MPa	E_f GPa	ε_{uf} %	f_u MPa	f_y MPa	E_s GPa	f_{uw} MPa	f_{yw} MPa
986	95.8	1.0	575	26.1	2.2	600	430	200	463	342

Note: [a] Values provided by manufacturers.

Table 2: Summary of test parameters

Group	Sign. of beams	b_w mm	b_f mm	h_f mm	h mm	L mm	a mm	a/d_e	d_p mm	ρ_s %	ρ_{sw} %	ρ_p %	Material of fiber	Number of FRP layers	w_f mm	s_f mm	t_f mm	ρ_f %
	P-A0-2.3						950	2.3					-	-	-	-	-	-
	P-A1-2.3-C						950	2.3					Carbon	1	75	150	1.0	0.83
	P-A1-2.3-G						950	2.3					Glass	1	75	150	1.3	1.08
A	P-A1-2.3-C-Cont	120	300	80	500	3500	950	2.3	362.5	1.32	0.16	0.38	Glass	1	830	Cont	1.3	2.17
	P-A1-2.3-G-Cont						950	2.3					Carbon	1	830	Cont	1.0	1.66
	P-A2-2.3-C						950	2.3					Carbon	2	75	150	2.0	1.66
	P-A2-1.9-C						800	1.9					Carbon	2	75	150	2.0	1.66
	P-A2-1.5-C						650	1.5					Carbon	2	75	150	2.0	1.66
	P-B0-2.3						950	2.3					-	-	-	-	-	-
	P-B1-2.3-C						950	2.3					Carbon	1	75	150	1.0	0.83
B	P-B1-2.3-G	120	300	80	500	3500	950	2.3	362.5	1.32	0.16	0.38	Glass	1	75	150	1.3	1.08
	P-B1-2.3-G-Cont						950	2.3					Glass	1	830	Cont	1.3	2.17
	P-B1-2.3-C-Cont						950	2.3					Carbon	1	830	Cont	1.0	1.66
	P-B2-2.3-C						950	2.3					Carbon	2	75	150	2.0	1.66
	P-C0-2.3						950	2.3					-	-	-	-	-	-
	P-C1-2.3-C						950	2.3					Carbon	1	75	150	1.0	0.83
	P-C1-2.3-G						950	2.3					Glass	1	75	150	1.3	1.08
C	P-C1-2.3-G-Cont	120	300	80	500	3500	950	2.3	362.5	1.32	0.16	0.38	Glass	1	830	Cont	1.3	2.17
	P-C1-2.3-C-Cont						950	2.3					Carbon	1	830	Cont	1.0	1.66
	P-C2-2.3-C						950	2.3					Carbon	2	75	150	2.0	1.66
	P-C2-1.9-C						800	1.9					Carbon	2	75	150	2.0	1.66
	P-C2-1.5-C						650	1.5					Carbon	2	75	150	2.0	1.66

Table 3: Test results

Group	Sign. of beams	$f_{c,cube}$ MPa	$f_{sp,cube}$ MPa	$P_{cr,fl}$ kN	$P_{cr,sh}$ kN	$P_{u,deb}$ kN	$P_{u,tot,exp}$ kN	$\delta_{u,mid}$ mm	$\varepsilon_{cu,pld}$ ‰	$\varepsilon_{cu,mid}$ ‰	$\varepsilon_{FRP,u}$ ‰	ε_{wu} ‰	$\varepsilon_{su,mid}$ ‰	$\varepsilon_{su,end}$ ‰	$\varepsilon_{pu,mid}$ ‰	$\varepsilon_{pu,end}$ ‰	Crack angle degree	Failure mode
A	P-A0-2.3			120	180	-	510	12.05	3.10	0.98	-	15.53	2.21	1.70	7.58	7.40	25.6	Shear
	P-A1-2.3-C			120	210	480	551	13.02	3.04	1.12	5.37	8.19	2.25	1.76	7.64	7.44	28.4	Shear
	P-A1-2.3-G			120	210	465	540	12.75	2.98	1.35	5.97	9.36	2.31	1.73	7.66	7.47	26.3	shear
	P-A1-2.3-G-Cont.	38.3	3.9	135	225	535	583	13.91	3.18	1.10	4.66	10.47	2.49	1.83	7.78	7.60	32.3	Shear
	P-A1-2.3-C-Cont.			150	-	555	608	15.18	3.27	1.11	2.29	9.87	2.45	1.81	7.70	7.52	33	Shear
	P-A2-2.3-C			150	240	480	573	13.78	3.11	1.20	2.73	9.46	2.50	1.79	7.61	7.42	31.9	Shear
	P-A2-1.9-C			165	255	530	666	13.25	3.21	1.13	2.62	9.56	2.58	1.80	7.69	7.51	33	Shear
	P-A2-1.5-C			210	360	635	735	12.15	3.37	1.06	2.07	11.77	2.63	1.83	7.75	7.58	38.8	Shear
B	P-B0-2.3			135	210	-	579	13.28	3.23	0.97	-	16.72	2.36	1.71	7.59	7.39	27.4	Shear
	P-B1-2.3-C			135	240	500	630	14.87	2.97	1.10	6.70	9.97	2.42	1.77	7.72	7.52	32.6	Shear
	P-B1-2.3-G	55.5	6.9	135	225	480	615	14.15	2.96	1.30	7.05	10.43	2.54	1.73	7.69	7.52	31.5	Shear
	P-B1-2.3-G-Cont.			150	255	535	669	15.97	3.16	1.09	5.04	10.64	2.78	1.84	7.89	7.70	35.1	Shear
	P-B1-2.3-C-Cont.			165	-	560	693	17.34	3.18	1.29	2.62	11.48	2.86	1.83	7.82	7.64	36.1	Shear
	P-B2-2.3-C			150	285	510	655	15.85	3.07	1.10	3.01	10.05	2.59	1.82	7.69	7.52	35.7	Shear
C	P-C0-2.3			150	210	-	661	15.05	3.42	0.94	-	17.82	2.72	1.70	7.67	7.51	28.7	Shear
	P-C1-2.3-C			150	255	645	735	17.58	2.85	1.06	7.21	12.83	2.90	1.77	7.82	7.62	34.2	Shear
	P-C1-2.3-G			150	270	600	706	16.54	2.90	1.19	8.55	13.46	2.96	1.80	7.77	7.61	33.2	Shear
	P-C1-2.3-G-Cont.	73.4	8.6	165	270	725	798	22.57	3.01	1.05	5.52	14.14	3.30	1.96	7.95	7.75	36.5	Shear
	P-C1-2.3-C-Cont			165	-	765	836	25.60	3.13	1.26	3.64	12.80	3.39	2.00	7.88	7.67	37.7	Shear
	P-C2-2.3-C			165	315	600	784	22.15	2.88	0.99	4.47	12.57	2.71	1.72	7.81	7.62	35.8	Shear
	P-C2-1.9-C			225	405	720	881	17.90	3.17	0.93	3.19	13.76	2.77	1.76	7.85	7.69	37.1	Shear
	P-C2-1.5-C			270	450	800	990	15.75	3.29	0.90	2.99	14.23	2.83	1.83	7.93	7.77	40.3	Shear

Table 4: Evaluation of the proposed formula

Ref.	Sign. of beams	b_w	a	d_s	d_p	d_e	a/d_e	L	f_c'	ρ_s	ρ_{sw}	ρ_p	f_{pc}	ρ_f	$V_{u,exp}$	$V_{u,theor}$	$V_{u,theor}/V_{u,exp}$
		mm	mm	mm	mm	mm		mm	MPa	%	%	%	MPa	%	kN	kN	
Kang and Ary, 2012	IB5	102	1143	425	457	435	2.63	4572	61.0	2.15	0.20	0.27	3.42	1.47	162	146	0.90
	IB10	102	1143	425	457	435	2.63	4572	61.0	2.15	0.20	0.27	3.42	0.74	119	143	1.20
Murphy et al., 2012	T3-12-Control	152	3660	1130	978	1083	3.38	9748	61.3	3.53	0.31	0.68	9.56	-	1125	936	0.83
	T3-12-S90-NA	152	3660	1130	914	1076	3.40	9748	61.4	3.53	0.31	0.68	9.56	0.29	1205	1082	0.90
	T3-12-S90-NA-PC#	152	3660	1130	914	1076	3.40	9748	65.3	3.53	0.31	0.68	9.56	0.29	1063	1104	1.04
Rupf et al., 2013[a]	SR21	150	4800	728	554	679	7.07	7200	30.8	1.37	0.09	0.19	2.40	-	399	446	1.12
	SR22	150	4800	728	554	679	7.07	7200	33.7	1.37	0.13	0.19	2.38	-	459	473	1.03
	SR23	150	4800	728	554	679	7.07	7200	35.3	1.37	0.06	0.19	2.45	-	364	464	1.27
	SR24	150	4800	728	554	680	7.06	7200	31.3	1.37	0.25	0.19	2.38	-	579	503	0.87
	SR25	150	4800	726	529	625	7.67	7200	33.1	0.98	0.09	0.38	4.73	-	484	537	1.11
	SR26	150	4800	726	529	625	7.67	7200	36.9	0.98	0.06	0.38	4.82	-	457	555	1.22
	SR27	150	4800	726	529	627	7.66	7200	28.3	0.98	0.19	0.38	4.85	-	606	558	0.92
	SR29	150	4800	728	554	681	7.05	7200	29.8	1.37	0.25	0.19	2.36	-	585	493	0.84
	SR31	150	4800	731	554	603	7.96	7200	31.3	0.99	0.09	0.97	2.93	-	309	373	1.21
Herbrand and Classen, 2015[a]	TB1-L	170	2000	575	323	385	5.19	5500	36.9	0.31	0.13	0.30	2.00	-	403	396	0.98
	TB1-R	170	2000	575	323	385	5.19	5500	36.9	0.31	0.07	0.30	2.00	-	314	369	1.18
	TB2-L	170	2000	575	287	315	6.34	5500	38.6	0.31	0.13	0.91	3.50	-	366	393	1.07
	TB2-R	170	2000	575	287	315	6.34	5500	38.6	0.31	0.07	0.91	3.50	-	328	362	1.10
	TB3-L	170	2000	575	287	315	6.34	5500	39.6	0.31	0.13	0.91	4.50	-	418	438	1.05
	TB3-R	170	2000	575	287	315	6.34	5500	36.9	0.31	0.07	0.91	4.50	-	337	392	1.16
Nguyen et al., 2015	B0	150	730	258	200	238	3.07	1660	50.0	1.69	0.23	0.44	3.44	-	160	184	1.15
	B0-1.9SF	150	730	258	200	238	3.07	1660	50.0	1.69	0.23	0.44	3.60	0.19	186	229	1.23
	B0-0.6SFa	150	730	258	200	238	3.07	1660	50.0	1.69	0.23	0.44	3.55	0.06	185	200	1.08
Nguyen et al., 2016	B1	150	730	258	200	238	3.07	1660	50.0	1.69	0.23	0.44	3.97		166	196	1.18
	B0-1.1SF	150	730	258	200	238	3.07	1660	50.0	1.69	0.23	0.44	3.32	0.11	178	205	1.16
	B0-1.9SF	150	730	258	200	238	3.07	1660	50.0	1.69	0.23	0.44	3.60	0.19	186	229	1.23
	B0-0.6SF	150	730	258	200	238	3.07	1660	50.0	1.69	0.23	0.44	3.55	0.06	185	200	1.08
	B0-1.0CF	150	730	258	200	238	3.07	1660	50.0	1.69	0.23	0.44	3.58	0.15	224	220	0.98
	B1-0.9SFb	150	730	258	200	238	3.07	1660	50.0	1.69	0.23	0.44	3.82	0.09	238	213	0.89

[a] The calculated values were converted from the proposed model of calculation to the author's testing scheme

Table 4 (continued)

Ref.	Beam	b_w	a	d_s	d_p	d_e	a/d_e	L	f_c'	ρ_s	ρ_{sw}	ρ_p	f_{pc}	ρ_f	$V_{u,exp}$	$V_{u,theor}$	$V_{u,theor}/V_{u,exp}$
		mm	mm	mm	mm	mm		mm	MPa	%	%	%	MPa	%	kN	kN	
Qi et al., 2016	S-1	120	1110	448	414	437	2.54	3600	58.3	1.33	0.39	0.17	1.84	-	204	214	1.05
	S-4	120	1262	448	414	437	2.89	3600	57.1	1.33	0.39	0.17	1.52	-	190	186	0.98
	S-6	120	1110	448	414	437	2.54	3600	50.5	1.33	0.39	0.17	1.52	-	217	193	0.89
	S-7	120	1110	448	414	437	2.54	3600	57.8	1.33	0.24	0.17	1.59	-	163	189	1.16
	S-8	120	1110	448	410	436	2.55	3600	51.9	1.33	0.39	0.17	1.64	-	173	184	1.07
	S-9	120	1110	448	459	451	2.46	3600	51.3	1.33	0.39	0.17	1.71	-	180	208	1.15
Current study	P-A0-2.3	120	950	455	363	406	2.34	3200	30.6	1.32	0.16	0.38	4.41	-	255	223	0.87
	P-B0-2.3	120	950	455	363	406	2.34	3200	44.4	1.32	0.16	0.38	4.41	-	290	252	0.87
	P-C0-2.3	120	950	455	363	406	2.34	3200	58.7	1.32	0.16	0.38	4.41	-	331	276	0.84
	P-A1-2.3-C	120	950	455	363	406	2.34	3200	30.6	1.32	0.16	0.38	4.41	0.83	276	263	0.95
	P-A1-2.3-G	120	950	455	363	406	2.34	3200	30.6	1.32	0.16	0.38	4.41	1.08	270	246	0.91
	P-A1-2.3-G-Cont	120	950	455	363	406	2.34	3200	30.6	1.32	0.16	0.38	4.41	2.17	292	268	0.92
	PA1-2.3-C-Cont	120	950	455	363	406	2.34	3200	30.6	1.32	0.16	0.38	4.41	1.67	304	302	0.99
	P-A2-2.3-C	120	950	455	363	406	2.34	3200	30.6	1.32	0.16	0.38	4.41	1.67	287	278	0.97
	P-A2-1.9-C	120	800	455	363	406	1.97	3200	30.6	1.32	0.16	0.38	4.41	1.67	333	308	0.92
	P-A2-1.5-C	120	650	455	363	406	1.60	3200	30.6	1.32	0.16	0.38	4.41	1.67	368	349	0.95
	P-B1-2.3-C	120	950	455	363	406	2.34	3200	44.4	1.32	0.16	0.38	4.41	0.83	315	309	0.98
	P-B1-2.3-G	120	950	455	363	406	2.34	3200	44.4	1.32	0.16	0.38	4.41	1.08	308	277	0.90
	P-B1-2.3-G-Cont	120	950	455	363	406	2.34	3200	44.4	1.32	0.16	0.38	4.41	2.17	335	303	0.91
	P-B1-2.3-C-Cont	120	950	455	363	406	2.34	3200	44.4	1.32	0.16	0.38	4.41	1.67	347	367	1.06
	P-B2-2.3-C	120	950	455	363	406	2.34	3200	44.4	1.32	0.16	0.38	4.41	1.67	328	331	1.01
	P-C1-2.3-C	120	950	455	363	406	2.34	3200	58.7	1.32	0.16	0.38	4.41	0.83	368	352	0.96
	P-C1-2.3-G	120	950	455	363	406	2.34	3200	58.7	1.32	0.16	0.38	4.41	1.08	353	304	0.86
	P-C1-2.3-G-Cont	120	950	455	363	406	2.34	3200	58.7	1.32	0.16	0.38	4.41	2.17	399	332	0.83
	P-C1-2.3-C-Cont	120	950	455	363	406	2.34	3200	58.7	1.32	0.16	0.38	4.41	1.67	418	428	1.02
	P-C2-2.3-C	120	950	455	363	406	2.34	3200	58.7	1.32	0.16	0.38	4.41	1.67	392	381	0.97
	P-C2-1.9-C	120	800	455	363	406	1.97	3200	58.7	1.32	0.16	0.38	4.41	1.67	441	423	0.96
	P-C2-1.5-C	120	650	455	363	406	1.60	3200	58.7	1.32	0.16	0.38	4.41	1.67	495	479	0.97

Prestressed beams strengthening by FRP U-sheets

Mean: **0.99**

Coefficient of Variation (COV): **0.11**

Prestressed beams

Mean: **1.04**

Coefficient of Variation (COV): **0.13**

Table 5: Comparison of the proposed formula and existing formulas from design codes

Ref.	Sign of beams	d_s	d_p	d_e	L	f_c'	f_{pc}	$V_{u,d,prop}$	$V_{u,ACI}$	$V_{u,CNR-DT}$	$V_{u,exp}$	$V_{u,d,prop}/V_{u,exp}$	$V_{u,ACI}/V_{u,exp}$	$V_{u,CNR-DT}/V_{u,exp}$
		mm	mm	mm	mm	MPa	MPa	kN	kN	kN	kN			
Kang and Ary, 2012	IB5	425	457	435	4572	61.0	3.42	99	117	120	162	0.61	0.72	0.74
	IB10	425	457	435	4572	61.0	3.42	96	111	100	119	0.81	0.93	0.84
Murphy et al., 2012	T3-12-Control	1130	978	1083	9748	61.3	9.56	633	387	550	1125	0.56	0.34	0.49
	T3-12-S90-NA	1130	914	1076	9748	61.4	9.56	731	581	941	1205	0.61	0.48	0.78
	T3-12-S90-NA-PC#	1130	914	1076	9748	65.3	9.56	746	582	953	1063	0.70	0.55	0.90
Rupf et al., 2013[a]	SR21	728	554	679	7200	30.8	2.40	302	147	144	399	0.76	0.37	0.36
	SR22	728	554	679	7200	33.7	2.38	320	167	165	459	0.70	0.36	0.36
	SR23	728	554	679	7200	35.3	2.45	313	137	138	364	0.86	0.38	0.38
	SR24	728	554	680	7200	31.3	2.38	340	224	220	579	0.59	0.39	0.38
	SR25	726	529	625	7200	33.1	4.73	363	136	169	484	0.75	0.28	0.35
	SR26	726	529	625	7200	36.9	4.82	375	126	163	457	0.82	0.28	0.36
	SR27	726	529	627	7200	28.3	4.85	377	182	209	606	0.62	0.30	0.34
	SR29	728	554	681	7200	29.8	2.36	333	224	218	585	0.57	0.38	0.37
	SR31	731	554	603	7200	31.3	2.93	252	131	133	309	0.82	0.42	0.43
Herbrand and Classen, 2015[a]	TB1-L	575	323	385	5500	36.9	2.00	267	183	110	403	0.66	0.45	0.27
	TB1-R	575	323	385	5500	36.9	2.00	250	154	89	314	0.80	0.49	0.28
	TB2-L	575	287	315	5500	38.6	3.50	266	158	107	366	0.73	0.43	0.29
	TB2-R	575	287	315	5500	38.6	3.50	245	129	90	328	0.75	0.39	0.28
	TB3-L	575	287	315	5500	39.6	4.50	296	159	115	418	0.71	0.38	0.28
	TB3-R	575	287	315	5500	36.9	4.50	265	129	97	337	0.79	0.38	0.29
Nguyen et al., 2015	B0	258	200	238	1660	50.0	3.44	125	45	79	160	0.78	0.28	0.49
	B0-1.9SF	258	200	238	1660	50.0	3.60	155	88	102	186	0.83	0.47	0.55
	B0-0.6SFa	258	200	238	1660	50.0	3.55	135	59	92	185	0.73	0.32	0.50
Nguyen et al., 2016	B1	258	200	238	1660	50.0	3.97	132	45	81	166	0.79	0.27	0.49
	B0-1.1SF	258	200	238	1660	50.0	3.32	139	71	83	178	0.78	0.40	0.47
	B0-1.9SF	258	200	238	1660	50.0	3.60	155	88	102	186	0.83	0.47	0.55
	B0-0.6SF	258	200	238	1660	50.0	3.55	135	59	92	185	0.73	0.32	0.50
	B0-1.0CF	258	200	238	1660	50.0	3.58	149	79	109	224	0.66	0.35	0.49
	B1-0.9SFb	258	200	238	1660	50.0	3.82	144	66	97	238	0.60	0.28	0.41

[a] The calculated values were converted from the proposed model of calculation to the author's testing scheme.

Table 5 (continued)

Ref.	Sign of beams	d_s	d_p	d_e	L	f_c'	f_{pc}	$V_{u,d,prop}$	$V_{u,ACI}$	$V_{u,CNR-DT}$	$V_{u,exp}$	$V_{u,d,prop}/V_{u,exp}$	$V_{u,ACI}/V_{u,exp}$	$V_{u,CNR-DT}/V_{u,exp}$
		mm	mm	mm	mm	MPa	MPa	kN	kN	kN	kN			
Qi et al., 2016	S-1	448	414	437	3600	58.3	1.84	144	155	135	204	0.71	0.76	0.66
	S-4	448	414	437	3600	57.1	1.52	126	147	132	190	0.66	0.77	0.69
	S-6	448	414	437	3600	50.5	1.52	130	154	130	217	0.60	0.71	0.60
	S-7	448	414	437	3600	57.8	1.59	128	127	104	163	0.78	0.78	0.64
	S-8	448	410	436	3600	51.9	1.64	124	154	131	173	0.72	0.89	0.76
	S-9	448	459	451	3600	51.3	1.71	140	165	135	180	0.78	0.91	0.75
Current test	P-A0-2.3	455	363	406	3200	30.6	4.41	151	99	88	255	0.59	0.39	0.35
	P-B0-2.3	455	363	406	3200	44.4	4.41	170	101	94	290	0.59	0.35	0.33
	P-C0-2.3	455	363	406	3200	58.7	4.41	187	103	99	331	0.56	0.31	0.30
	P-A1-2.3-C	455	363	406	3200	30.6	4.41	177	151	138	276	0.64	0.55	0.50
	P-A1-2.3-G	455	363	406	3200	30.6	4.41	166	129	118	270	0.61	0.48	0.44
	P-A1-2.3-G-Cont	455	363	406	3200	30.6	4.41	181	158	144	292	0.62	0.54	0.49
	PA1-2.3-C-Cont	455	363	406	3200	30.6	4.41	204	203	182	304	0.67	0.67	0.60
	P-A2-2.3-C	455	363	406	3200	30.6	4.41	188	171	158	287	0.66	0.60	0.55
	P-A2-1.9-C	455	363	406	3200	30.6	4.41	208	-	158	333	0.62	-	0.47
	P-A2-1.5-C	455	363	406	3200	30.6	4.41	236	-	158	368	0.64	-	0.43
	P-B1-2.3-C	455	363	406	3200	44.4	4.41	209	167	153	315	0.66	0.53	0.49
	P-B1-2.3-G	455	363	406	3200	44.4	4.41	188	131	129	308	0.61	0.43	0.42
	P-B1-2.3-G-Cont	455	363	406	3200	44.4	4.41	205	160	160	335	0.61	0.48	0.48
	P-B1-2.3-C-Cont	455	363	406	3200	44.4	4.41	248	234	205	347	0.72	0.67	0.59
	P-B2-2.3-C	455	363	406	3200	44.4	4.41	224	193	177	328	0.68	0.59	0.54
	P-C1-2.3-C	455	363	406	3200	58.7	4.41	238	183	166	368	0.65	0.50	0.45
	P-C1-2.3-G	455	363	406	3200	58.7	4.41	206	133	139	353	0.58	0.38	0.39
	P-C1-2.3-G-Cont	455	363	406	3200	58.7	4.41	225	162	174	399	0.56	0.41	0.44
	P-C1-2.3-C-Cont	455	363	406	3200	58.7	4.41	289	263	225	418	0.69	0.63	0.54
	P-C2-2.3-C	455	363	406	3200	58.7	4.41	258	214	193	392	0.66	0.55	0.49
	P-C2-1.9-C	455	363	406	3200	58.7	4.41	285	-	193	441	0.65	-	0.44
	P-C2-1.5-C	455	363	406	3200	58.7	4.41	323	-	193	495	0.65	-	0.39
											Mean	**0.69**	**0.49**	**0.48**
											COV	**0.12**	**0.36**	**0.31**

Table 6: Evaluation the contribution of each individual component to the total shear resistance

Ref.	Sign. of beams	$V_{u,theor}$		Contribution of Concrete V_c		Contribution of Stirrups V_{sw}		Contribution of FRP sheets V_F		Contribution of Prestressing force V_p	
		kN	%	kN	%	kN	%	kN	%	kN	%
FRP-strengthened PC beams - unbonded straight tendons											
Current test	A1-2.3-C	263	100	161	61.1	29	11.2	73	27.7	-	-
	A1-2.3-G	246	100	175	71.1	29	11.9	42	16.9	-	-
	A1-2.3-G-Cont	268	100	156	58.1	29	10.9	83	31.0	-	-
	A1-2.3-C-Cont	302	100	127	42.2	29	9.7	145	48.1	-	-
	A2-2.3-C	278	100	148	53.2	29	10.6	101	36.3	-	-
	A2-1.9-C	308	100	178	57.8	29	9.5	101	32.7	-	-
	A2-1.5-C	349	100	219	62.7	29	8.4	101	28.9	-	-
	B1-2.3-C	309	100	187	60.4	29	9.5	93	30.1	-	-
	B1-2.3-G	277	100	207	74.5	29	10.6	42	15.0	-	-
	B1-2.3-G-Cont	303	100	191	62.9	29	9.7	83	27.4	-	-
	B1-2.3-C-Cont	367	100	151	41.2	29	8.0	186	50.8	-	-
	B2-2.3-C	331	100	173	52.2	29	8.9	129	38.9	-	-
	C1-2.3-C	352	100	211	59.8	29	8.3	112	31.9	-	-
	C1-2.3-G	304	100	233	76.7	29	9.6	42	13.6	-	-
	C1-2.3-G-Cont	332	100	220	66.2	29	8.8	83	25.0	-	-
	C1-2.3-C-Cont	428	100	174	40.7	29	6.9	224	52.4	-	-
	C2-2.3-C	381	100	197	51.5	29	7.7	155	40.8	-	-
	C2-1.9-C	423	100	238	56.3	29	6.9	155	36.8	-	-
	C2-1.5-C	479	100	294	61.4	29	6.1	155	32.5	-	-
Mean					**58.4**		**9.1**		**32.5**		
FRP-strengthened PC beams - bonded straight tendons											
Kang and Ary, 2012	IB5	146	100	91	62.7	37	25.6	17	11.7	-	-
	IB10	143	100	97	67.8	37	26.2	9	6.0	-	-
Murphy et al., 2012	T3-12-S90-NA	1122	100	594	52.9	239	21.3	289	25.7	-	-
	T3-12-S90-NA-PC#	1145	100	617	53.9	239	20.9	289	25.2	-	-
Nguyen et al., 2015	B0-1.9SF	229	100	168	73.4	-	-	61	26.6	-	-
	B0-0.6SFa	200	100	180	89.9	-	-	20	10.1	-	-
Nguyen et al., 2016	B0-1.1SF	205	100	169	82.2	-	-	36	17.8	-	-
	B0-1.9SF	229	100	168	73.4	-	-	61	26.6	-	-
	B0-0.6SF	200	100	180	89.9	-	-	20	10.1	-	-
	B0-1.0CF	220	100	171	77.9	-	-	49	22.1	-	-
	B1-0.9SFb	213	100	183	85.9	-	-	30	14.1	-	-
Mean					**59.3***		**23.5[b]**		**17.8[b]**		**-**

Note: [b] applicable to beams with stirrups only

Table 6 (continued)

Ref.	Sign. of beams	$V_{u,theor}$		Contribution of Concrete V_c		Contribution of Stirrups V_{sw}		Contribution of Fibers V_F		Contribution of Prestressing force V_p	
		kN	%	kN	%	kN	%	kN	%	kN	%
PC Beams - unbonded harped tendons											
Herbrand and Classen, 2015[a]	TB1-L	396	100	226	57.1	77	19.6	-	-	92	23.3
	TB1-R	369	100	239	64.6	39	10.5	-	-	92	24.9
	TB2-L	393	100	197	50.2	77	19.7	-	-	118	30.1
	TB2-R	362	100	205	56.7	39	10.7	-	-	118	32.7
	TB3-L	438	100	250	57.0	77	17.7	-	-	111	25.3
	TB3-R	392	100	246	62.9	39	9.9	-	-	107	27.2
Qi et al., 2016	S-1	214	100	79	37.1	93	43.6	-	-	41	19.3
	S-4	186	100	56	30.0	93	50.2	-	-	37	19.9
	S-6	193	100	63	32.6	93	48.4	-	-	37	19.0
	S-7	189	100	95	50.3	56	29.6	-	-	38	20.1
	S-9	208	100	95	45.6	93	44.9	-	-	20	9.5
Mean					**49.5**		**27.7**		**-**		**22.8**
PC Beams - unbonded straight tendons											
Qi et al., 2016	S-8	184	100	91	49.3	93	50.7	-	-	-	-
Current test	A0-2.3	223	100	194	86.8	29	13.2	-	-	-	-
	B0-2.3	252	100	223	88.4	29	11.6	-	-	-	-
	C0-2.3	276	100	247	89.4	29	10.6	-	-	-	-
Mean					**78.5**		**21.5**		**-**		**0.0**
PC Beams - bonded harped tendons											
Rupf et al., 2013[a]	SR21	446	100	255	57.1	55	12.3	-	-	137	30.6
	SR22	473	100	255	53.9	81	17.0	-	-	137	29.1
	SR23	464	100	282	60.9	40	8.7	-	-	141	30.5
	SR24	503	100	209	41.6	158	31.4	-	-	136	27.1
	SR25	537	100	268	50.0	55	10.2	-	-	214	39.9
	SR26	555	100	294	52.9	40	7.2	-	-	222	39.9
	SR27	558	100	229	41.1	118	21.1	-	-	211	37.8
	SR29	493	100	201	40.8	158	32.0	-	-	134	27.2
	SR31	373	100	237	63.5	50	13.3	-	-	87	23.2
Mean					**51.3**		**17.0**		**-**		**31.7**
PC Beams - bonded straight tendons											
Murphy et al., 2012	T3-12-Control	961	100	722	**75.1**	239	**24.9**	-	-	-	-
Nguyen et al., 2015	B0	184	100	184	100.0	-	-	-	-	-	-
Nguyen et al., 2016	B1	196	100	196	100.0	-	-	-	-	-	-
Mean					**75.1[b]**		**24.9[b]**	**-**		**-**		

Note: [a] the calculated values were converted from the proposed model of calculation to the author's testing scheme; [b] applicable to beams with stirrups only.